

ANNUAL  
REVIEWS **Further**

Click here to view this article's online features:

- Download figures as PPT slides
- Navigate linked references
- Download citations
- Explore related articles
- Search keywords

# Near-Inertial Internal Gravity Waves in the Ocean

Matthew H. Alford,<sup>1</sup> Jennifer A. MacKinnon,<sup>1</sup>  
Harper L. Simmons,<sup>2</sup> and Jonathan D. Nash<sup>3</sup>

<sup>1</sup>Scripps Institution of Oceanography, University of California, San Diego, La Jolla, California 92093; email: malford@ucsd.edu

<sup>2</sup>School of Fisheries and Ocean Sciences, University of Alaska at Fairbanks, Fairbanks, Alaska 99775

<sup>3</sup>College of Earth, Ocean, and Atmospheric Sciences, Oregon State University, Corvallis, Oregon 97331

Annu. Rev. Mar. Sci. 2016. 8:95–123

First published online as a Review in Advance on August 26, 2015

The *Annual Review of Marine Science* is online at marine.annualreviews.org

This article's doi:  
10.1146/annurev-marine-010814-015746

Copyright © 2016 by Annual Reviews.  
All rights reserved

## Keywords

near-inertial waves, internal gravity waves, turbulence, mixing, climate

## Abstract

We review the physics of near-inertial waves (NIWs) in the ocean and the observations, theory, and models that have provided our present knowledge. NIWs appear nearly everywhere in the ocean as a spectral peak at and just above the local inertial period  $f$ , and the longest vertical wavelengths can propagate at least hundreds of kilometers toward the equator from their source regions; shorter vertical wavelengths do not travel as far and do not contain as much energy, but lead to turbulent mixing owing to their high shear. NIWs are generated by a variety of mechanisms, including the wind, nonlinear interactions with waves of other frequencies, lee waves over bottom topography, and geostrophic adjustment; the partition among these is not known, although the wind is likely the most important. NIWs likely interact strongly with mesoscale and submesoscale motions, in ways that are just beginning to be understood.

## 1. INTRODUCTION

Near-inertial waves (NIWs), or internal gravity waves with a frequency near the inertial frequency  $f$ , are a dominant mode of high-frequency variability in the ocean, appearing as a prominent peak rising well above the Garrett & Munk (1975) continuum internal wave spectrum (**Figure 1**). Unlike these background internal waves, NIWs often have a preferred propagation direction that is at times linked to a source near the surface. At their most active, they dominate kinetic energy, with velocities reaching up to  $1 \text{ m s}^{-1}$  following hurricanes and typhoons (Firing et al. 1997). They are recognizable by their characteristic circularly polarized velocities (**Figure 2**) and their strong shear (**Figures 3** and **4**). Because of the latter, they are likely a major contributor to upper-ocean mixing, which can affect a variety of processes, including biogeochemistry and climate (Jochum et al. 2012).

NIWs share some important characteristics with the other most energetic aspect of the internal wave spectrum, the internal tides. Both have similar power input to them on the global scale (Egbert & Ray 2000, Alford 2003a) and therefore have similar potential to contribute to ocean variability and turbulent mixing. Both can propagate far from their source regions before breaking (Ray & Mitchum 1996, Alford 2003a, Zhao & Alford 2009). However, NIWs are far more intermittent (Fu 1981), are generally higher mode (Silverthorne & Toole 2009, Alford 2010), and have smaller

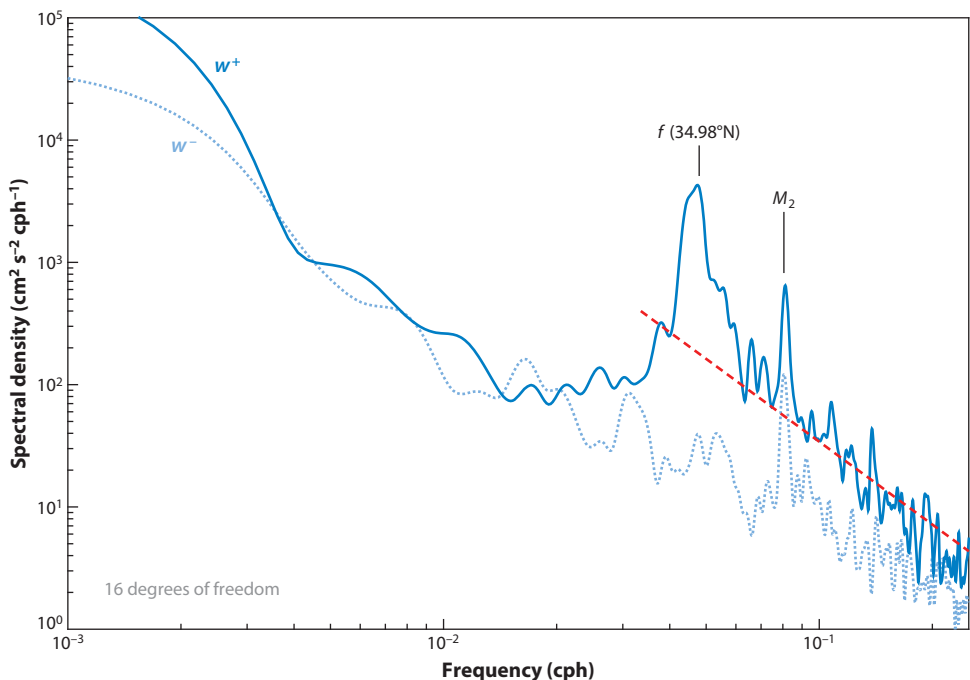


**Figure 1**

Rotary velocity spectrum at 261-m depth from current-meter data from the WHOI699 mooring gathered during the WESTPAC1 experiment (mooring at 6,149-m depth.) The solid blue line ( $w^+$ ) is clockwise motion, and the dashed blue line ( $w^-$ ) is counterclockwise motion; the differences between these emphasize the downward energy propagation that often dominates the near-inertial band. The dashed red line is the line  $E_0 N \omega^{-p}$  with  $N = 2.0$  cycles per hour (cph),  $E_0 = 0.096 \text{ cm}^2 \text{ s}^{-2} \text{ cph}^{-2}$ , and  $p = 2.25$ , which is quantitatively similar to levels in the Cartesian spectra presented by Fu (1981) for station 5 of the Polygon Mid-Ocean Experiment (POLYMODE) II array.

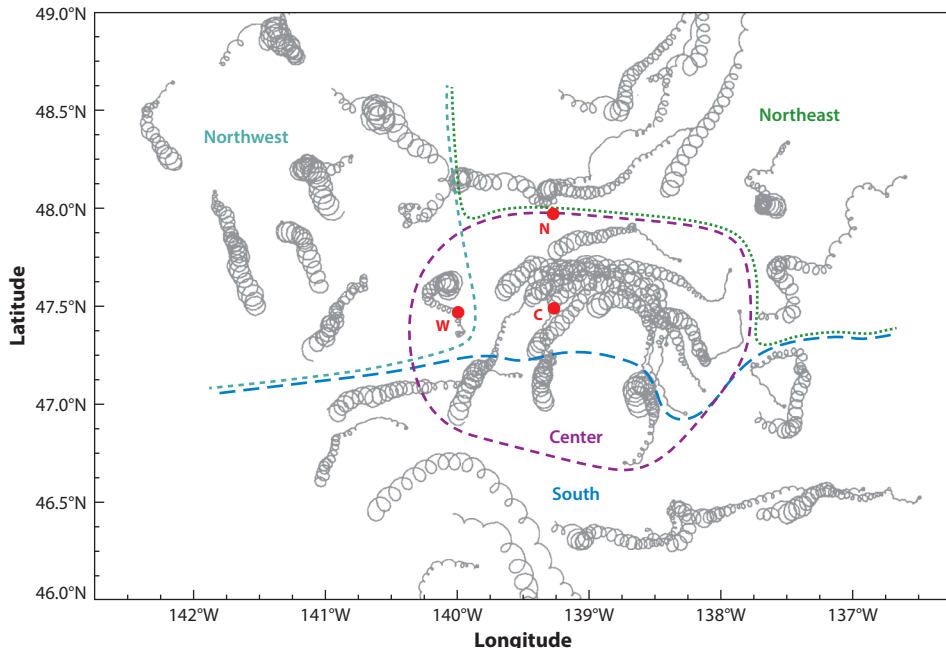


**Figure 2**

Drifter tracks in the Ocean Storms Experiment, showing near-inertial trajectories following a midlatitude storm. The dashed lines represent geographic regions: center (purple), northeast (green), northwest (teal), and south (blue). The red dots are moorings (C, center; N, north; W, west). Modified from D'Asaro et al. (1995).

vertical displacements for the same energy. These attributes make them more difficult to observe in some ways than internal tides, so that somewhat less is known about them. Importantly, owing to their comparatively slower group velocities, NIWs likely interact more strongly with the mesoscale than internal tides, complicating propagation paths. This, combined with the fact that NIWs have several generation mechanisms, makes their characterization challenging.

The last review of NIWs was the pioneering work by Fu (1981), which focused on a set of moorings in the Atlantic collected during the Polygon Mid-Ocean Dynamics Experiment (POLYMODE). Fu concluded that the inertial peak could arise from “local” forcing (waves generated in the vicinity of the observation location at a frequency near  $f$ ) and/or “remote” forcing (higher-frequency waves that have propagated poleward to where they are near the local inertial frequency). He developed a turning-point theory for the latter, obtaining fair agreement with observations. Since then, the groundbreaking Ocean Storms Experiment (D'Asaro et al. 1995), theoretical work (Garrett 2001), and observations of dominantly equatorward propagation (Alford 2003a) have suggested that wind-generated NIWs originate locally near  $f$ ; the high-wavenumber aspects remain in the region because they propagate slowly, whereas low-mode remote motions propagate hundreds of kilometers equatorward (rather than poleward) from their source and therefore appear in spectra somewhat above the local inertial frequency. Since Fu's (1981) review, the additional complicating role of mesoscale motions on NIWs has been (incompletely) explored and the list of additional candidate generation mechanisms besides wind forcing has been refined, although their relative importance remains unknown.

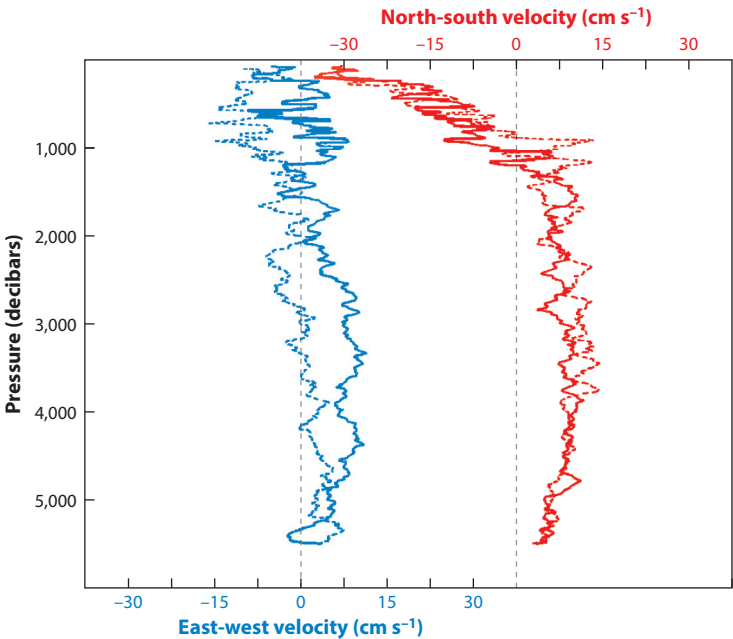


**Figure 3**

Two profiles (dashed and solid lines) of east-west (blue) and north-south (red) velocity taken at an interval of half an inertial period, showing high-wavenumber near-inertial motions. Modified from Leaman & Sanford (1975).

This article first reviews the basic physics of NIWs and then presents a necessarily incomplete history of the observations and modeling that have led to our current state of knowledge. We discuss the basic characteristics and spatial and temporal scales of NIWs, followed by their observed global patterns. We then review their various generation mechanisms and the evidence for each, followed by observations of their mixing and their interaction with mesoscale currents. We conclude with a discussion of unanswered questions and research directions.

## 2. DEFINITIONS AND THEORY

NIWs are solutions to the linearized hydrostatic Boussinesq equations of motion on an *f* plane, which can be written as

$$\begin{aligned}
 \frac{\partial u}{\partial t} &= -\frac{1}{\rho_0} \frac{\partial p}{\partial x} + fv + \frac{1}{\rho_0} \frac{\partial}{\partial z} \tau_x, \\
 \frac{\partial v}{\partial t} &= -\frac{1}{\rho_0} \frac{\partial p}{\partial y} - fu + \frac{1}{\rho_0} \frac{\partial}{\partial z} \tau_y, \\
 \frac{\partial p}{\partial z} &= -g\rho', \\
 \nabla \cdot \mathbf{u} &= 0, \\
 \frac{\partial \rho'}{\partial t} &= \frac{\rho_0}{g} N^2 w,
 \end{aligned} \tag{1}$$

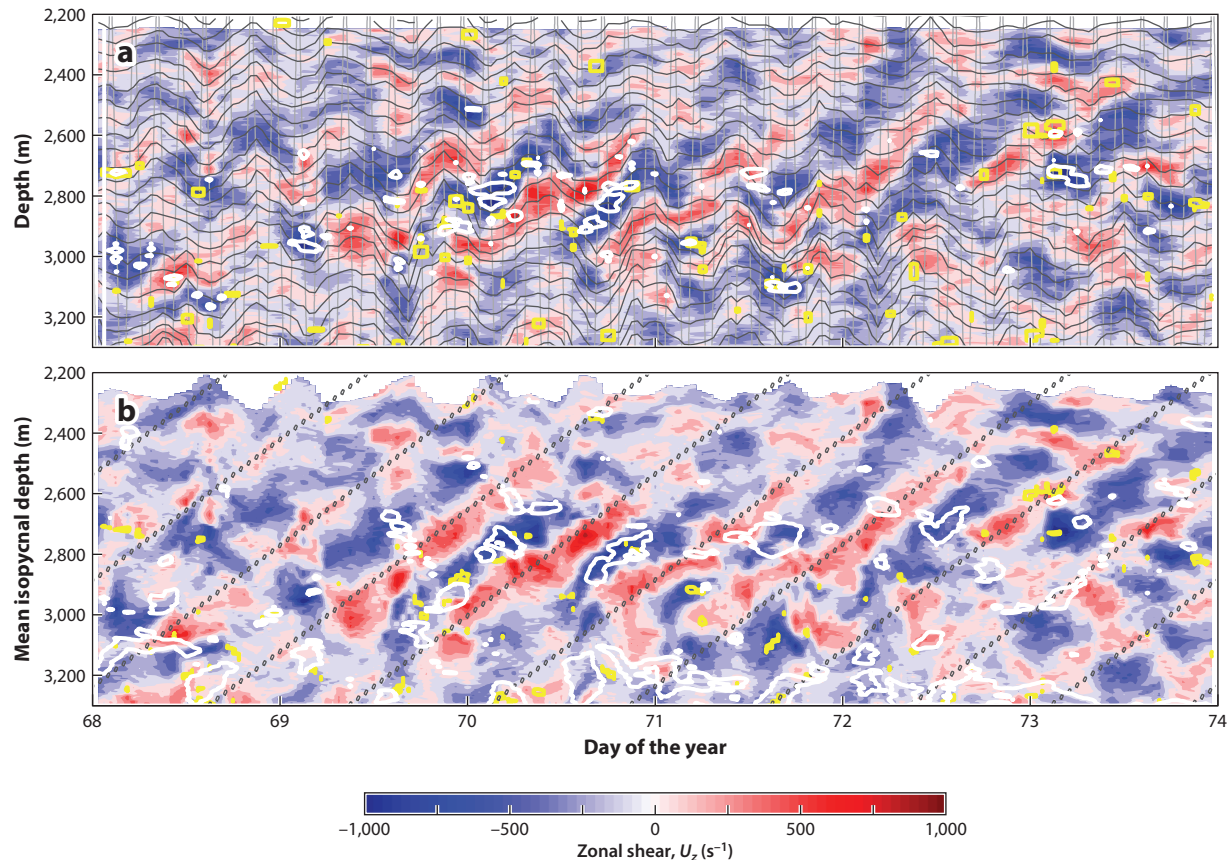


**Figure 4**

Zonal shear plotted versus (a) depth and (b) density (expressed as the mean depth of each isopycnal), showing the upward phase propagation of near-inertial shear layers. Shear layers are aligned with isopycnals (dark gray lines in panel a), which are heaved vertically by internal waves of other frequencies (primarily tidal; light gray lines); this heaving is removed in the isopycnal-following frame (panel b). The dissipation rate from overturns is contoured in yellow (contour value  $1.5 \times 10^{-8} \text{ W kg}^{-1}$ ); the Richardson number (white contours) drops below 0.8 once per wave period. In panel b, the dotted lines represent the wave phase for a signal with  $\omega = 1.03 f$  and  $\lambda = 350 \text{ m}$ . Modified from Alford (2010).

where  $\rho' (x, y, z, t)$  is the perturbation density difference from a mean density  $\overline{\rho(z)}$ , and  $N^2 = -(g/\rho_0)(\partial \bar{\rho}/\partial z)$  is the background stratification. At the surface of the ocean, the horizontal vector  $(\tau_x, \tau_y)$  is interpreted as the wind stress, whereas in the interior of the fluid, this turns into a viscous stress term that is typically neglected when considering NIW propagation (at least until waves dissipate; see Section 7). Note that we also make the so-called traditional approximation, considering only the component of the Coriolis term that is aligned with the local vertical,  $f = (2\Omega \times \mathbf{u}) \cdot \hat{z}$ , neglecting the locally horizontal component of the Earth's rotation (but this may be invalid near turning latitudes; Gerkema & Shrira 2005, Winters et al. 2011). Within the surface mixed layer (where momentum is sometimes assumed to be mixed instantaneously), and neglecting preexisting pressure gradients, the effect of wind stress can be considered using a simplified form

## NEAR-INERTIAL WAVES NEAR COASTS

Many of the assumptions made in this article are violated near coasts, because the boundary limits the spatial scales in one direction and the shallow depth introduces complications (such as bottom drag) that can cause coupling between modes (MacKinnon & Gregg 2005). Because of the shallow depths, coastal NIWs tend to be dominated by the first few modes; NIW energy decreases toward the coastal wall (Shearman 2005) to satisfy the boundary condition that no horizontal motion occurs there. The mixing that NIWs drive can be particularly important in supplying nutrients to coastal ecosystems, as demonstrated by Lucas et al. (2014). Because diurnal sea breezes are intensified near coasts, these winds become an important driver, particularly near 30° latitude, where the inertial period is approximately once per day (Lerczak et al. 2001, Nam & Send 2013). NIWs have also been observed in submarine canyons (Chinn et al. 2012), where the canyon walls disrupt the usual circular rotation, leading to nearly rectilinear motion; the dynamics of such canyon-modified NIWs have not been adequately explored.

of the horizontal momentum equations above:

$$\begin{aligned}\frac{\partial U}{\partial t} &= +fV + \frac{1}{\rho_0} \frac{\partial}{\partial z} T_x, \\ \frac{\partial V}{\partial t} &= -fU + \frac{1}{\rho_0} \frac{\partial}{\partial z} T_y,\end{aligned}\quad (2)$$

where the uppercase variables are depth-averaged versions of the lowercase variables in Equation 1. Solutions to this so-called slab model are the sum of a steady Ekman transport to the right of the wind and anticyclonic circular motions at the local inertial frequency,  $f$  (Pollard & Millard 1970, Gill 1982, D'Asaro 1985). Note that these equations are not valid in the presence of a lateral boundary, such as coasts (see sidebar Near-Inertial Waves Near Coasts).

As a limiting case within the ocean interior, one can neglect the stress terms from Equation 1 and assume wavelike solutions to all variables, e.g.,

$$u(x, y, z, t) = \hat{u} e^{i(kx+ly+mz-\omega t)}, \quad (3)$$

where  $(k, l, m)$  is a three-dimensional wave vector and  $\omega$  is the wave frequency. Insertion into Equation 1 produces a dispersion relation that must be satisfied for propagating wave solutions to exist:

$$\omega^2 = f^2 + N^2 \frac{(k^2 + l^2)}{m^2} = f^2 + \frac{N^2 k_H^2}{m^2}, \quad (4)$$

where  $k_H^2 = k^2 + l^2$ . Again, this is the hydrostatic limit, a good approximation given the near-horizontal aspect ratio of NIWs. As with all internal waves, group propagation is perpendicular to phase propagation, so that upward phase propagation indicates downward energy propagation (as in the example in **Figure 4**). Of particular interest below, the vertical component of group speed for frequencies close to  $f$  is

$$C_{gz} = \frac{\partial \omega}{\partial m} \approx \frac{-N^2 k_H^2}{m^3 f}. \quad (5)$$

For example, for a typical observed vertical wavelength of 350 m and  $\omega = 1.03 f$ , as in **Figure 4**, the horizontal wavenumber would be approximately 80 km and the vertical group velocity approximately  $10^{-3}$  m s<sup>-1</sup> (86 m d<sup>-1</sup>). It is clear from Equation 5 that for the small-vertical-wavelength motions (large  $m$ ), vertical group velocity becomes very slow. Additionally, the horizontal wavenumber and group speed are both quite sensitive to  $\omega$ , which is generally not

known very precisely for finite-length time series. And because NIWs are typically observed in short packets, it is often difficult to define  $\omega$  with a high degree of accuracy.

The above derivations are formally valid only on an  $f$  plane. If waves are allowed to propagate a considerable meridional distance, additional complications arise in association with the  $\beta$  effect (Garrett 2001), where  $\beta = \partial f / \partial y$ . In particular, if waves propagate to a turning latitude in which their frequency approaches  $f$ , application of Equation 4 requires motions to have an infinitely large horizontal scale—or, rather, an infinitely large horizontal-to-vertical aspect ratio. This is often referred to as a turning latitude, as ray-tracing theory predicts poleward-propagating waves to turn and return equatorward here (Section 5). Solutions on a  $\beta$  plane around this latitude may instead be described by Airy functions (Munk & Phillips 1968).

### 3. BASIC CHARACTERISTICS OF NEAR-INERTIAL WAVES

NIWs have been observed for many decades, beginning in 1930 with Ekman. According to Webster (1968), Ekman initially interpreted his observations at 30° latitude as diurnal tides but later concluded that they were inertial oscillations (Ekman 1953). The advent of the moored current meter at Woods Hole Oceanographic Institution in the 1960s gave rise to many more observations of near-inertial currents (reviewed in Webster 1968). These currents were nearly always clockwise polarized in the Northern Hemisphere as expected, and were usually much more temporally intermittent than internal tides.

Leaman & Sanford (1975) analyzed vertical profiles of velocity that were separated in time by approximately half an inertial period (**Figure 3**) and further deduced that NIWs have vertical scales of 100–300 m and tend to rotate clockwise with depth, consistent with downward energy propagation (see sidebar General Characteristics of Near-Inertial Waves). Near-inertial motions in the mixed layer (**Figure 2**) cause float trajectories to trace out approximate circles superimposed on background flows (D’Asaro et al. 1995).

More recent observations, including those using acoustic Doppler current profilers (ADCPs), vertically profiling microstructure instruments, and moored profilers (Doherty et al. 1999), significantly increased the time resolution of vertical profiles. For example, moored profilers measured an NIW propagating downward past 3,000 m near the Mendocino Escarpment (Alford 2010) (**Figure 4**). The shear was clockwise polarized, with phase lines slanted upward in time, indicating downward energy propagation. Vectors rotated clockwise in depth, also indicative of downward propagation (Leaman & Sanford 1975). The layers were advected vertically by other motions, notably the internal tide, as first noted by Sherman (1989). Plotting shear on isopycnals (**Figure 4b**) substantially straightens these out. As opposed to pure inertial motions that are horizontal, slightly super-inertial motions have vertical displacements that modulate the stratification via the wave strain (white contours in **Figure 4**) and thus the water column stability, which is important for mixing (Section 7).

#### GENERAL CHARACTERISTICS OF NEAR-INERTIAL WAVES

The general characteristics of NIWs are as follows:

- Clockwise and counterclockwise polarization in the Northern and Southern Hemispheres, respectively
- Frequency of  $1\text{--}1.2f$
- Shear peak at a vertical wavelength of 100–400 m
- Lateral scale of 10–100 km

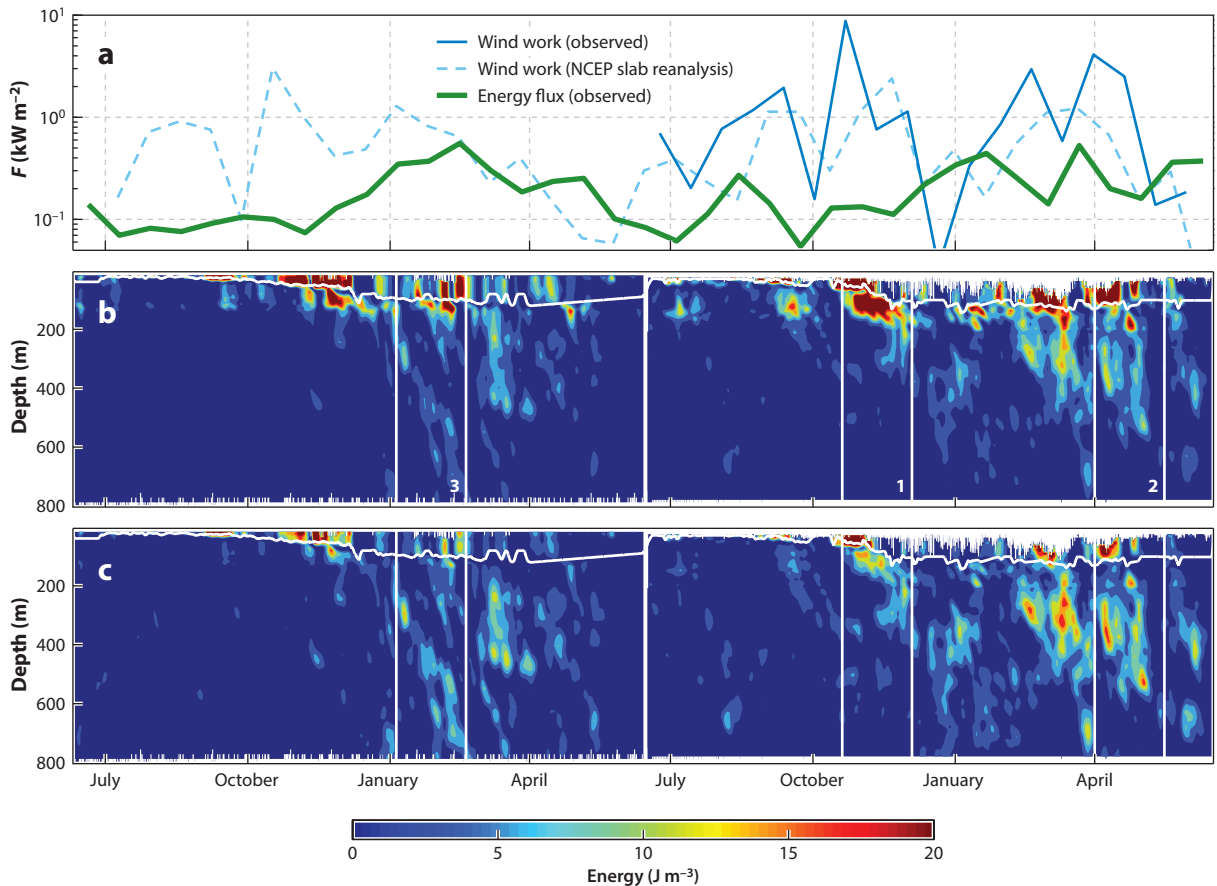


**Figure 5**

Near-inertial waves at Ocean Station Papa. (a) Wind work from observations (solid blue line) and from Equation 2 forced with reanalysis winds (dashed blue line), along with observed energy flux computed as the mean of energy from 600 to 800 m multiplied by  $c_{gz} = 1.03 \times 10^{-4} \text{ m s}^{-1}$  ( $9 \text{ m d}^{-1}$ ; thick green line). All three lines have been smoothed over 20 days. (b) Near-inertial kinetic energy for the whole two-year record. (c) The same as panel b but additionally accounting for WKB refraction. In panels b and c, the mixed-layer depth is overplotted in white. Abbreviations: NCEP, National Centers for Environmental Prediction; WKB, Wentzel, Kramers, Brillouin. Modified from Alford et al. (2012).

An oft-noted aspect of NIWs is their intermittency or strong time variability (e.g., Fu 1981) in comparison with internal tides or the internal wave continuum, the latter of which is much more constant in time and space. A two-year time series of NIW kinetic energy collected at Ocean Station Papa in the northeast Pacific (Figure 5b) shows a clear annual cycle as well as numerous “events” lasting 5–20 inertial periods. Both of these are consistent with generation by storms, a known forcing mechanism (discussed below).

Internal waves propagating vertically through a depth-dependent stratification  $N(z)$  refract, with their wavelength and amplitude changing according to WKB (Wentzel, Kramers, Brillouin) theory such that energy  $\sim N$ . In a climatology constructed from approximately 2,200 historical current-meter records, adjusting for this effect shows that NIW energy decreases only very slowly with depth (Alford & Whitmont 2007). Clear seasonal cycles exist at all depths (Figure 6) and all extratropical latitudes, again highlighting the importance of wind forcing. The kinetic energy is

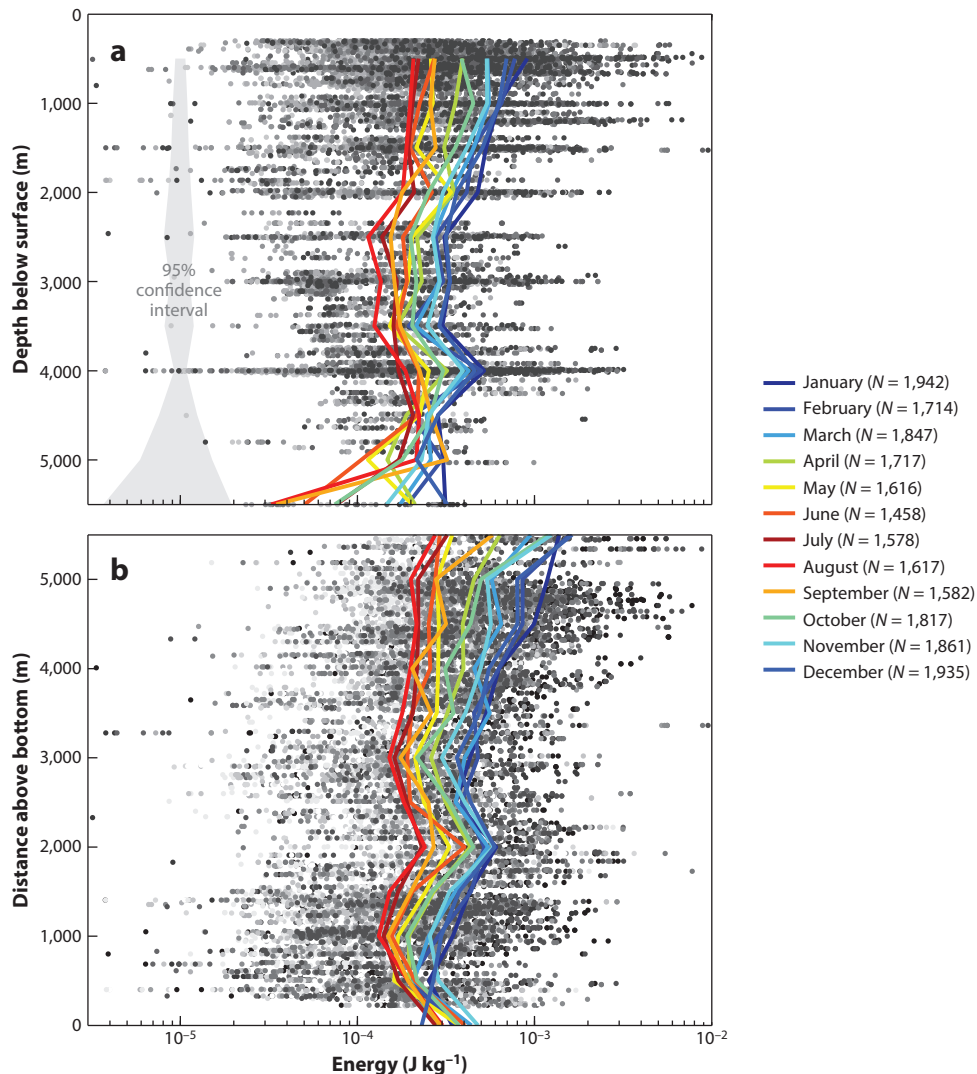


**Figure 6**

Northern Hemisphere WKB-scaled near-inertial kinetic energy plotted versus (a) depth below the surface and (b) distance above the bottom. Individual 30-day estimates are plotted with dots, with lighter shades for summer months. Colored lines indicate the 500-m boxcar average for each month; the legend additionally indicates the number of observations in each month. The gray area on the left side of panel *a* shows the 95% confidence intervals on the mean computed using the number of observations in each depth range.

Abbreviation: WKB, Wentzel, Kramers, Brillouin. Modified from Alford & Whitmont (2007).

$(1\text{--}10) \times 10^{-4} \text{ J kg}^{-1}$ , or several centimeters per second in these monthly averages; speeds can be at least an order of magnitude greater for several days following storms.

Although useful for many purposes, discrete current meters at single depths cannot define the spatial structure of NIWs. ADCP or profiling data are needed to characterize the vertical structure of NIWs, which often have wavelengths of 100–400 m (Figures 2 and 4). Vertical wavenumber spectra of shear, which accentuate the higher vertical wavenumbers compared with velocity spectra,

often show a hump in this wavenumber range above the white GM76 spectrum (Garrett & Munk 1975, Cairns & Williams 1976). Observations of lateral structure are rare, but at times show gently sloping shear layers that can be coherent for tens of kilometers (A. Pickering, M.H. Alford, Z. Zhao, J.A. MacKinnon, R. Pinkel & J.M. Klymak, manuscript in preparation). With time series of profiles (such as those from a moored profiler or ADCP), both the spectral hump and the sloping layers can be unambiguously identified with NIWs (Pinkel 1985; Silverthorne & Toole 2009; B.S. Chinn, J.B. Girton & M.H. Alford, manuscript in preparation; A. Pickering, M.H. Alford, Z. Zhao, J.A. MacKinnon, R. Pinkel & J.M. Klymak, manuscript in preparation).

Although potentially important for mixing, these high-wavenumber aspects of the near-inertial band contain little energy compared with that in the first few modes (Leaman & Sanford 1975, Silverthorne & Toole 2009, Alford 2010). This is important because the long vertical wavelengths and high propagation speeds of low modes enable them to travel far from their sources. In this regard, NIWs resemble internal tides, which can propagate more than 3,500 km from their sources (Ray & Mitchum 1996, Zhao & Alford 2009) and are believed in general to radiate the bulk of their energy to the far field. Using the small subset of approximately 80 moorings in the above-mentioned current-meter database that had sufficient vertical resolution to resolve modes 1 and 2, Alford (2003a) showed that NIWs have an energy and energy flux similar to those of internal tides and also radiate appreciable fractions of their energy from sources. The error bars are greater and the number of measurements are much fewer for NIWs than for internal tides for two primary reasons: (a) They are much more intermittent than internal tides, and (b) they have frequencies much closer to  $f$  and therefore have much smaller vertical displacements for the same energy (i.e., the ratio of kinetic to potential energy is much greater for NIWs). Both of these aspects preclude the detection of NIWs by satellite altimetry, which has proved so useful for the study of internal tides (Ray & Mitchum 1996, Zhao & Alford 2009, Zhao et al. 2012). Modeling efforts are beginning to be quite useful and are discussed below.

## 4. GENERATION

Because of the resonance at  $f$  in the equations of motion, nearly any forcing will excite near-inertial motions. The most important mechanisms appear to be the wind blowing on the ocean surface, nonlinear wave-wave interactions, lee-wave formation by geostrophic flow over seafloor topography, and spontaneous emission through loss of balance. Wind generation has by far the most observational support, but the relative importance of the others is not known. Here, we review each of these mechanisms.

### 4.1. Wind

Wind stress impulses or fluctuations with frequencies in the near-inertial band can resonantly force inertial motions in the surface mixed layer via Equation 2. Traveling midlatitude storms (D'Asaro 1985), hurricanes (Firing et al. 1997), and typhoons (Yang & Hou 2014) all contain strong inertially rotating components. Additionally, diurnal sea breezes are resonant near 30° latitude (Lerczak et al. 2001), whereas equatorial weather timescales resonantly match the inertial frequency of several days at very low latitudes (Mickett et al. 2010). Once these motions are excited, horizontal convergences and divergences then pump the stratified base of the mixed layer, generating internal waves near the local inertial frequency. As shown schematically in Figure 7, these waves are then free to radiate downward into the stratified interior, draining energy from the mixed layer, transferring it to waves of other frequencies via wave-wave interactions, and ultimately depositing it in the form of turbulent mixing. Because the waves are generated near

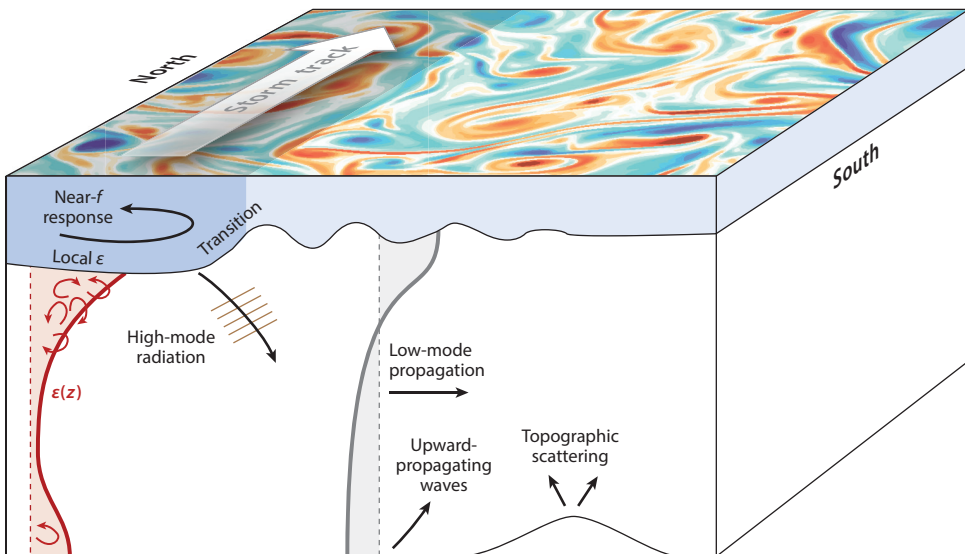


**Figure 7**

Schematic showing processes associated with near-inertial generation, dissipation, and propagation. As storms move along the storm track (*thick white arrow*), a local response occurs with frequencies near the local Coriolis frequency. Both high- and low-mode internal gravity waves are excited. High modes propagate along curving characteristics downward and equatorward. The higher modes have strong shear that results in mixing,  $\epsilon(z)$ . Low-mode wave radiation (indicated in gray) takes the form of oscillations that propagate equatorward. Upward characteristics and topographic scattering have been observed, but the processes involved are not completely understood. Modified from Simmons & Alford (2012).

their turning latitude, propagation is predominantly toward the equator (Anderson & Gill 1979, Alford 2003a).

Gill (1984) developed a modal formalism for describing the subsequent excitation of sub-mixed-layer motions. Essentially, the slab velocity profile (motion in the mixed layer and none below) is projected onto the dynamical modes (Gill 1982) computed for the prestorm stratification. The energy projects predominantly on the lowest modes (a red spectrum), with the actual spectrum determined by the mixed-layer depth and the stratification (Gill 1984). As the modes propagate away, energy propagates downward into the ocean interior (see Figures 5 and 7); alternatively, the propagation can be described in terms of rays (Kroll 1975, Zervakis & Levine 1995).

The initial atmospheric forcing of the mixed layer occurs over many hundreds of kilometers, the typical synoptic scales of midlatitude storms. The initial puzzle with Gill's (1984) work was that internal waves imprinted with these horizontal scales propagate into the ocean very slowly (timescales of  $\sim 1$  year) because group velocity is inversely proportional to wavelength (Equation 5). Instead, several processes act to decrease the scales of coherence of mixed-layer motions, allowing the generation of waves with shorter horizontal wavelengths that can propagate into the stratified interior. One dominant process is clearly the variation of inertial frequency with latitude, the so-called  $\beta$  effect (D'Asaro 1989) (Figure 8), although mesoscale eddies may also play a role (Weller 1982) (see also Section 6). Mixed-layer motions at different latitudes oscillate at slightly different frequencies, so in the days following a storm passage, motions at slightly different latitudes dephase from each other, leading the meridional scale of coherence to shrink to less than 100 km.

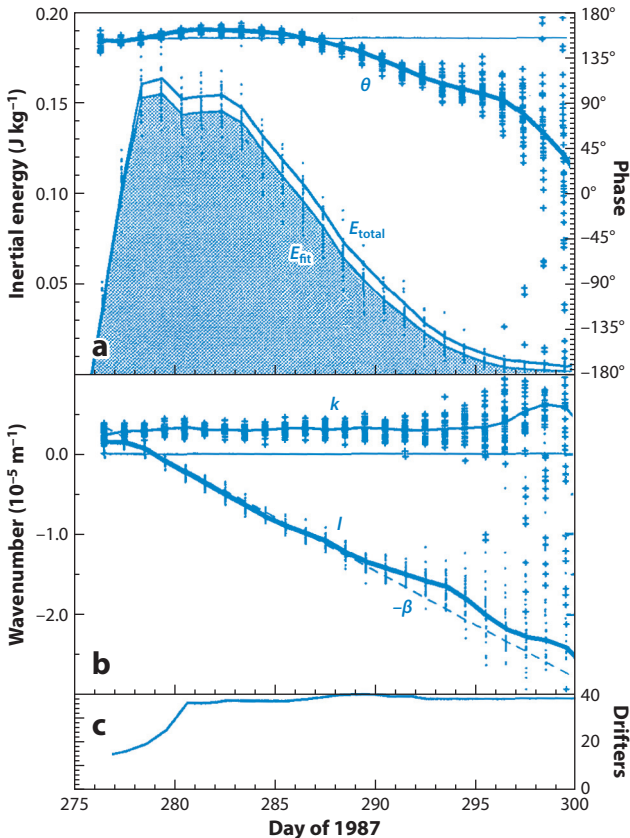


**Figure 8**

Evolution of mixed-layer energy and wavenumber following a storm. (a) Demodulated phase (blue line) and kinetic energy (thin blue line and blue shading) computed from drifters. (b) Zonal wavenumber  $k$  and meridional wavenumber  $l$ , showing the decrease of  $l$  with  $\beta t$ . (c) Number of observations used in the calculation. Modified from D’Asaro et al. (1995).

In the groundbreaking Ocean Storms Experiment (see **Figure 2**), D’Asaro et al. (1995) and D’Asaro (1995a,b) showed that much of this physics is correct. In particular, this work clearly demonstrated the role of the  $\beta$  effect in leading to the initial growth of horizontal wavenumbers. Writing an inertial plane wave on a  $\beta$  plane ( $f = f_0 + \beta y$ ) as  $e^{i(l_0y - ft)} = e^{i[(l_0 - \beta t)y - f_0t]}$  shows that the initial meridional wavenumber  $l_0$  becomes more negative as  $\beta t$  increases; observations show a remarkable agreement with this simple prediction (**Figure 8b**). Once the lateral scales are reduced to  $O(100 \text{ km})$ , modes begin to propagate more rapidly, and energy decays (**Figure 8a**). This scenario is qualitatively consistent with lateral radiation of the first two modes from the region. However, there was approximately a factor-of-two discrepancy between this simple estimate and the observed decay. Additionally, Gill’s formalism could not reproduce the observed “beam” wherein energy migrated quickly downward with time from the mixed layer following storm events (for a more recent example of downward-propagating energy at the same location, see **Figure 5**).

An important consequence is that neither the decay of mixed-layer motions nor the rate of energy transfer into the deep ocean can adequately be predicted for the best-documented storm

## NEAR-INERTIAL WAVE GENERATION BY TYPHOONS AND HURRICANES

Tropical storms are particularly efficient generators of NIWs owing to their strong wind stresses and their compact size, which leads to more rapid propagation. Following theoretical work by Price et al. (1994), several studies have documented the NIW wakes of hurricanes and typhoons (e.g., Firing et al. 1997, Sanford et al. 2011, Yang & Hou 2014). The response is similar to that of a midlatitude storm in some ways, but vertical propagation is more rapid owing to the smaller lateral scales of tropical storms. Globally, K. Emanuel (personal communication) has estimated a total wind work of 0.05 TW, ~10% of the total, and furthermore notes the importance of mixing at the base of the mixed layer caused by inertial motions in giving rise to the observed “cold wake” of hurricanes, which is visible in sea surface temperature imagery (Emanuel 2001).

response on record. This conundrum has remained for the 25 years since these data were collected, largely because the Ocean Storms data lacked sufficient vertical resolution to quantify the vertical mode structure and the associated modal transfers. The complicating influence of the mesoscale field, which causes similar wind events to have very different depth penetration (**Figure 5**), is another source of uncertainty, which is discussed in Section 6.

The pioneering work of D’Asaro (1985) provided the first estimates of the work done by the wind on inertial motions in the mixed layer, taking advantage of the demonstrated skill of the slab mixed-layer model developed by Pollard & Millard (1970). Starting with Equation 2, D’Asaro (1985) derived an energy equation for the mixed-layer motions from which the work done by the wind can be computed. These slab model calculations are attractive because they predict the inertial velocity in the mixed layer such that the work can be computed from estimates of wind stress and climatological mixed-layer depth alone. A series of global calculations ensued (Alford 2001, 2003b; Watanabe & Hibiya 2002; Jiang et al. 2005; Rimac et al. 2013), giving estimates between 0.3 and 1.5 TW for the total rate of wind work through the ocean surface; much of the spread can likely be attributed to different wind products. Jiang et al. (2005), for example, obtained results from 0.5 to 1.5 TW depending on the spatial and temporal resolution of the wind products used; Rimac et al. (2013) obtained a similar range by varying the spatial resolution of the wind forcing. Typhoons and hurricanes (see sidebar Near-Inertial Wave Generation by Typhoons and Hurricanes) are thought to possibly contribute an additional 10% (Alford 2001; K. Emanuel, personal communication). Additional uncertainty and possible biases of up to a factor of four arise from the inability of the slab model to correctly characterize rapidly deepening mixed layers (Plueddemann & Farrar 2006); rare comparisons of wind work computed from the slab model and directly from contemporaneous velocity and wind measurements (Plueddemann & Farrar 2006, Alford et al. 2012) are probably insufficient to estimate the degree of the bias.

Model estimates of global wind work, which do not assume a slab model but are still subject to wind-product uncertainties as well as the mixed-layer parameterizations they employ, range from 0.3 TW (Simmons & Alford 2012) (**Figure 9**) to 0.5 TW (Furuichi et al. 2008). The state of the art appears to be that although the exact amount of work done by the wind on inertial motions is uncertain by at least a factor of two to three, even the lower estimates are comparable to the other sources of internal waves (~1 TW; Egbert & Ray 2000) and lee waves (~0.2 TW; Nikurashin & Ferrari 2011). Interest in all of these components persists because they constitute a substantial fraction of the 2 TW thought to be needed in order to maintain the abyssal stratification (Munk & Wunsch 1998, Waterhouse et al. 2014).

The spatial distribution of wind forcing from a global model (**Figure 9**) resembles previous slab model calculations, showing strong inputs in the western portion of each basin in midlatitudes

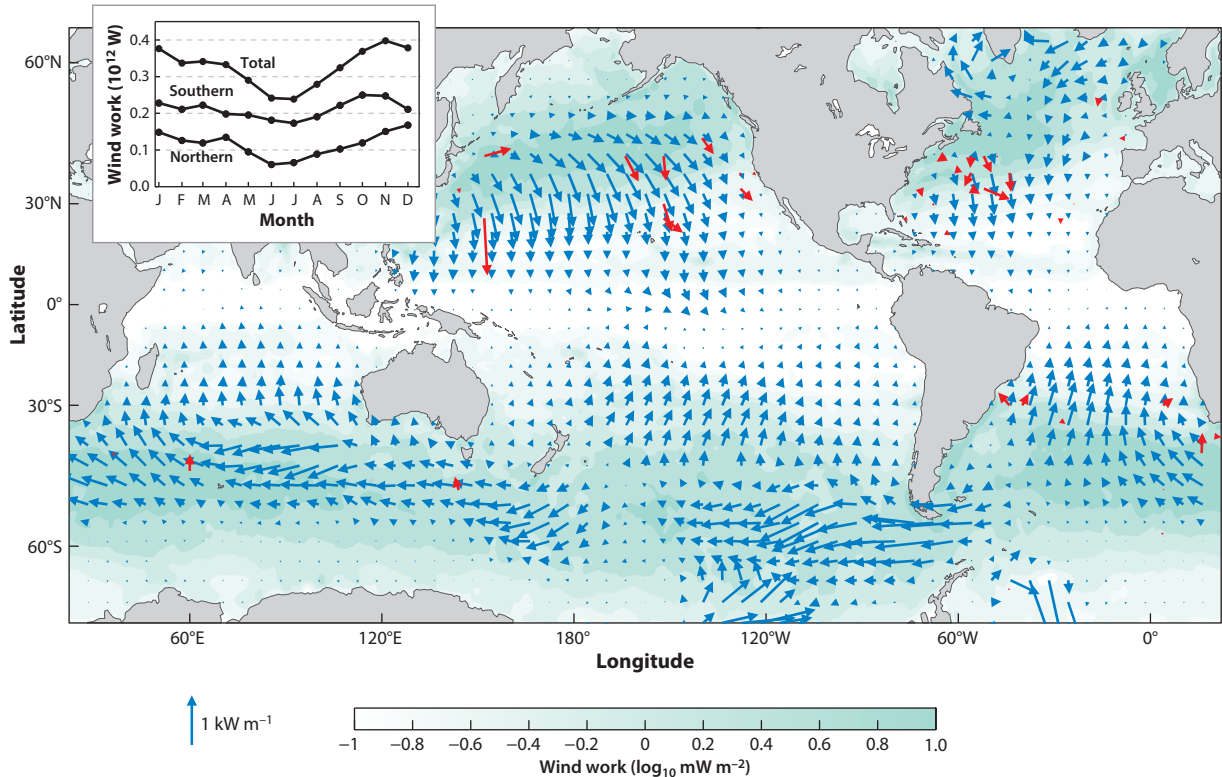


**Figure 9**

Modeled (blue arrows) and observed (red arrows) horizontal energy fluxes in the first vertical mode. The modeled values are from 2007; the observations span 20 years of measurements. The inset shows the hemispherically and globally integrated wind work computed from the model. The aqua color shows the annual-mean distribution of the work, illustrating the enhancement under storm tracks. Modified from Simmons & Alford (2012).

and a peak in winter (Figure 9 inset), which confirms that midlatitude storms provide the bulk of the wind work. The general distribution of wind work closely matches the observed near-inertial energy in the mixed layer from drifters (Chaigneau et al. 2008) (Figure 10).

#### 4.2. Parametric Subharmonic Instability and Other Wave-Wave Interactions

Weakly nonlinear interactions between internal waves have long been thought to transfer energy between motions with different wavenumbers and frequencies (McComas & Müller 1981, Müller et al. 1986). The interaction is often described in terms of triad theory, in which triads of waves may interact provided that the sums and differences of their frequencies combine to zero to provide secular growth/decay in the energy transfer terms. Parametric subharmonic instability (PSI) is a specific subclass of nonlinear wave-wave interaction that involves energy exchange between one low-mode (large vertical wavelength) wave and two higher-mode waves with opposite vertical wavenumber signs (one up-going, one down-going), each with close to half the forcing wave frequency. PSI has been posited as a potentially significant loss term for low-mode internal tides (MacKinnon & Winters 2005). The interaction is formally possible at latitudes where all three waves are still within the internal wave frequency band ( $f < \omega < N$ ), but it is thought to be

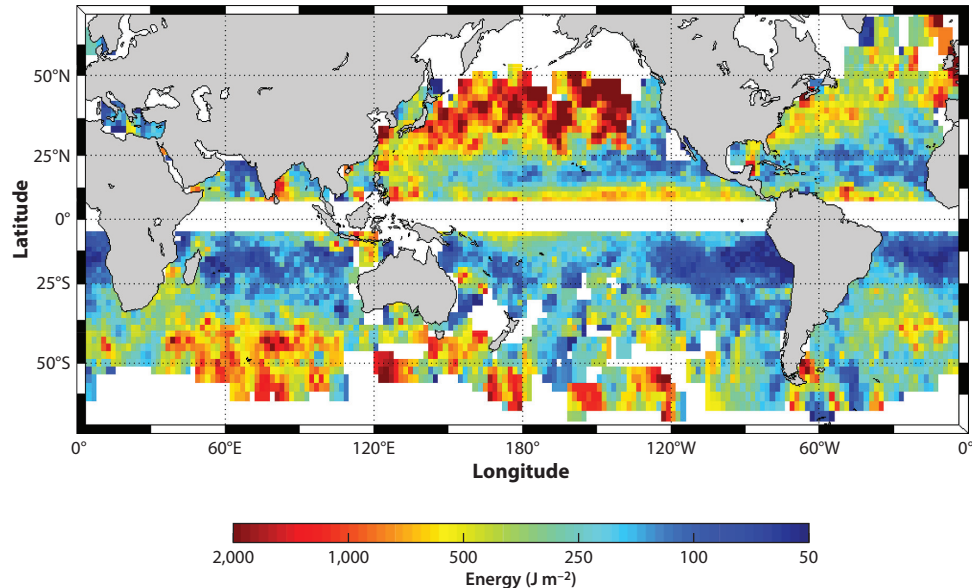


**Figure 10**

Mixed-layer inertial-band kinetic energy in late fall and early winter (October–December) measured from drifting floats. Modified from Chaigneau et al. (2008).

particularly effective near latitudes at which the subharmonic daughter waves are close to the local inertial frequency. For semidiurnal and diurnal internal tides, these interactions occur near latitudes of 29° and 14°, respectively.

Although this process was initially ruled out by Eden & Olbers (2014) as too slow to matter in an isotropic incoherent wave field, numerical simulations by MacKinnon & Winters (2005), Simmons (2008), and Hazewinkel & Winters (2011) suggested that it could in fact be more important for coherent low-mode internal tides, which are often found radiating away from tall, steep topography. Indeed, observations near 29°N (van Haren 2005, Carter & Gregg 2006, Alford et al. 2007, Chinn et al. 2012, MacKinnon et al. 2013, Sun & Pinkel 2013) and 14.4°N (Alford 2008) suggest that PSI is indeed active in the ocean. Although in situ estimates of energy transfer rates are modest (MacKinnon et al. 2013), near-inertial energy has been observed to increase toward the equator crossing the critical latitude (Alford et al. 2007); additionally, tidal loss estimated from altimetry (Tian et al. 2006) and parameterized diffusivity (E. Kunze, personal communication) both appear to peak at the critical latitudes. More generally, Lvov et al. (2012) demonstrated that in the type of broadband internal wave field that is ubiquitous in the world's oceans (e.g., Polzin & Lvov 2011), resonant and nonresonant nonlinear interactions consistently act to steadily transfer energy toward motions at the local inertial frequency. It is thus possible that modest but commonplace interactions of this sort partially explain the pervasive presence of high-mode NIWs with both up- and down-going group velocity throughout the ocean interior.

### 4.3. Lee Waves

Internal waves can be excited by steady or slowly evolving, low-frequency geostrophic flow impinging on seafloor topography, which in principle and in numerical models can develop into NIWs through a process elucidated by Nikurashin & Ferrari (2010a,b). In this mechanism, a

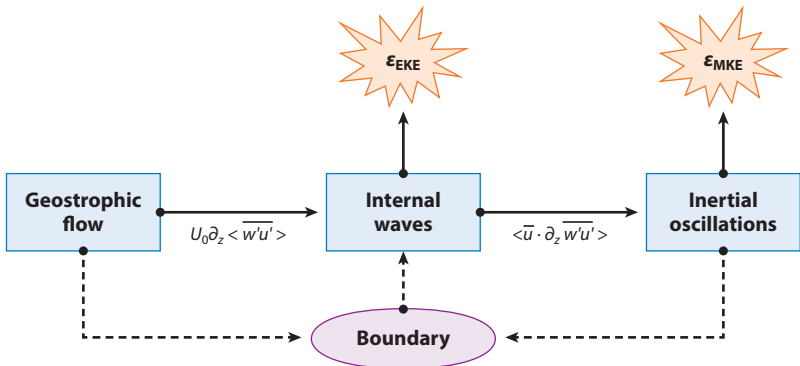


**Figure 11**

Mechanism for near-inertial wave generation from lee waves, showing the resultant growth rates and the terms involved. Modified from Nikurashin & Ferrari (2010b).

resonant feedback develops that produces NIWs with velocity amplitudes similar to those of the overlying geostrophic flow. Nikurashin & Ferrari (2010b) developed the theory for the process (represented schematically in **Figure 11**), which is initiated through classic lee-wave generation. As radiated internal waves deposit momentum nonuniformly into the overlying fluid, they induce spatially varying near-inertial oscillations. In turn, these oscillations alter near-bottom velocities and hence add time dependence to the lee-wave generation at the inertial frequency. For sufficient geostrophic flow and topographic amplitude, this feedback is strong enough that the overlying flow can saturate in timescales of less than a few days, making the energy transfer particularly efficient. Numerical simulations confirm the NIW growth rates and illustrate the feedback, which extracts significant energy from the geostrophic mean eddy kinetic energy, driving significant modeled energy dissipation over a region spanning  $O(1,000)$  m above the bottom.

Work on this pathway was motivated in part by its role as a potential sink of energy for the mesoscale (Ferrari & Wunsch 2009) and in part by the search for dissipation mechanisms for the wind input in the Southern Ocean. The Southern Ocean represents a significant fraction of global wind power because wind and current vectors are often aligned (Wunsch 1998), yet it lacks rigid lateral boundaries that can directly induce geostrophic eddy scattering and dissipation. Inferences from numerical simulations (Nikurashin et al. 2013) suggest that geostrophic energy dissipation is catalyzed by bottom topography interactions, with a significant fraction ( $\sim 20\%$ ) associated with wave radiation and dissipation within the ocean interior. Bottom boundary processes account for the remainder (Arbic et al. 2009). Observational evidence from Drake Passage (St. Laurent et al. 2012) indeed showed enhanced dissipation associated with rough topography. Numerical simulations (Nikurashin & Ferrari 2010b) forced using observed low-frequency velocity and density over realistic Southern Ocean topography showed dissipation rates that agreed with those observed, as well as the upward energy propagation expected for lee waves (St. Laurent et al. 2012). However, the process has yet to be directly observed, and it is difficult to ascertain what fraction of the geostrophic energy dissipation is associated with the lee waves themselves as opposed to the NIWs generated by them via nonlinear interactions. It is possible that the enhanced NIW energy within Drake Passage (e.g., Nowlin et al. 1986) is associated with lee-wave generation, but this direct connection has yet to be established. Additional anecdotal evidence of enhanced near-inertial shear variance and coinciding low-frequency flows near the Mid-Atlantic Ridge (Thurnherr et al. 2005, Toole 2007) may provide additional support for this mechanism. A search for direct observational evidence of this lee-wave mechanism seems warranted.

#### 4.4. Spontaneous Generation

Beginning with the classic Rossby (1938) adjustment problem, wherein slumping ageostrophic fronts radiate energy to infinity via inertial oscillations, mean and low-frequency flows have been recognized both as a possible source of energy for NIWs and as a sink for the mesoscale eddy field (Arbic et al. 2009, Ferrari & Wunsch 2009, Scott et al. 2011, Alford et al. 2013). Recent work has focused more on a general class of mechanisms collectively termed loss of balance, which are distinct from the Rossby adjustment problem in that there is a continual transfer of energy whenever geostrophic balance is not satisfied. Note that the transfer of energy to the NIWs distinguishes these mechanisms from trapping and other types of linear wave–mean flow interactions discussed in Section 6, which focus or trap NIWs but do not exchange energy with them.

A body of work suggests that, because of the timescale separation between the NIWs ( $\sim f^{-1}$ ) and the mean flows (given by the Rossby number,  $Ro$ ), the NIW growth rate is exponentially small for small  $Ro$  (for a nice review, see Vanneste 2012). However, the parameter space wherein NIWs interact with mesoscale and submesoscale flows is quite complex (Vanneste 2012). The mechanisms fall into two rough categories: frontogenesis (Hoskins & Bretherton 1972), in which NIWs arise as instabilities in a sharpening front formed by large-scale strain, and radiation by time-dependent instabilities of the low-frequency flow (Ford 1994). The importance of either type of mechanism is unknown; the only clear observations were made at the subtropical front in the North Pacific, where NIWs were seen radiating tens of kilometers away from a moderate front ( $Ro \sim 0.2\text{--}0.3$ ) (Alford et al. 2013). Wind forcing appeared to be an order of magnitude too weak to have generated the waves, implicating the front as a source. Modeling of these processes (Nagai et al. 2015) is beginning to provide some observable predictions but is still in its infancy. Hence, the magnitude of the source term for the NIWs is virtually unknown.

### 5. PROPAGATION

The possibility that NIWs can propagate long distances has been considered for some time, beginning with Munk & Phillips (1968), who demonstrated some of the complications arising from propagation on the  $\beta$  plane. Specifically, waves with  $\omega > f$  propagating toward the poles will reach a turning latitude where their meridional group velocity goes to zero. WKB theory can be used to show that their rays smoothly turn equatorward, although the theory is not valid very close to the turning latitude; Airy functions give the NIW structure there and poleward. Additionally, Gerkema & Shrira (2005) and Winters et al. (2011) have pointed out that the traditional approximation becomes invalid near the turning latitude. Here, using the full Coriolis term allows for propagation up to several hundred kilometers farther poleward, and in particular, the equations suggest that poleward-propagating NIWs may be preferentially funneled down to regions of low stratification in the abyss beyond this point, potentially producing locally enhanced dissipation (Winters et al. 2011). Two other important consequences of distant meridional propagation are the possibilities that (a) the entire NIW peak itself could arise from continuum waves  $\omega \gg f$  propagating poleward until they reach the local  $f$  (Fu 1981) and (b) NIWs generated near  $f$  could propagate equatorward until their frequency becomes  $2f$ , at which point they become unstable owing to parametric subharmonic instability (Niwa & Hibiya 1997, Nagasawa et al. 2000, Komori et al. 2008).

NIWs are at times thought of as high-mode disturbances propagating downward and equatorward along rays (Garrett 2001) (Figures 5 and 7) or as low modes propagating laterally (Figure 9). Although reality may be equivalently described as superpositions in either description, the ray/mode duality has led to some confusion in the literature. Given the potential for NIWs to contribute to deep mixing (Section 7), a natural question is how much of the wind work done at

the surface penetrates to depth. The redness of the modal spectrum ensures that some energy is immediately deposited at great depth (Gill 1984), likely explaining the observed seasonal cycle of energy even at depths of thousands of meters (Alford & Whitmont 2007, Silverthorne & Toole 2009) (**Figure 6**). On the other hand, although upper-ocean energy is usually predominantly downward, there is also a sizable upward-propagating high-mode contingent (Alford 2010; A. Pickering, M.H. Alford, Z. Zhao, J.A. MacKinnon, R. Pinkel & J.M. Klymak, manuscript in preparation). It is unknown whether these waves have propagated all the way from the surface to the bottom and then reflected/scattered or were generated at depth or at the bottom via lee waves.

Although they did not directly measure it, D'Asaro et al. (1995) concluded that the bulk of the energy leaves wind generation regions in the form of low-mode waves. In this regard, NIWs resemble internal tides, which also transmit most of their energy to great range (Rudnick et al. 2003, Alford et al. 2015). The first direct evidence for long-range propagation of NIWs was from historical moorings (Alford 2003a), which showed a time-mean energy flux of approximately  $0.5 \text{ kW m}^{-1}$  at most of the  $\sim 80$  sites examined (red arrows in **Figure 9**). Propagation was nearly always equatorward, as expected given generation near  $f$  on a  $\beta$  plane (Anderson & Gill 1979, Garrett 2001) and counter to the earlier alternative explanation of the near-inertial peak by Fu (1981). Simple and data-poor energy budget calculations in the North Pacific estimated that  $O(50\%)$  of the energy input into a control volume surrounding the storm track radiated past  $30^\circ\text{N}$  (Alford 2003a).

Subsequent model calculations by Furuichi et al. (2008) and Simmons & Alford (2012) upheld this general picture, and in fact found remarkable agreement with observations even though the observations were made in many different years (**Figure 9**). The ultimate fate of this energy is completely unknown.

## 6. INTERACTION OF NEAR-INERTIAL WAVES WITH THE MESOSCALE

Although the  $\beta$  effect (**Figure 8**) is undoubtedly an important process in allowing horizontal scales and wavelengths to shrink enough for waves to propagate, especially for low-mode waves, the variability in the ocean response for similar wind events at Ocean Station Papa (**Figure 5**) clearly implicates a role for other processes. As early as 1982, mesoscale eddies were identified as an obvious candidate (Weller 1982). NIWs typically have horizontal spatial scales on the order of 10–100 km (Fu 1981; A. Pickering, M.H. Alford, Z. Zhao, J.A. MacKinnon, R. Pinkel & J.M. Klymak, manuscript in preparation). Their slow group velocities make them likely to interact strongly with mesoscale features in the ocean. That interaction can take several forms, including mesoscale influence on the wind generation process, refraction and trapping of propagating waves, and two-way nonlinear energy transfers with mesoscale and submesoscale features such as fronts, all of which we discuss in this section.

### 6.1. Mesoscale Imprinting on Near-Surface Wave Generation

Mesoscale vorticity can organize the way wind energy is imparted to the surface by shifting the resonant frequency from the local  $f_o$  to the effective inertial frequency

$$f_{\text{eff}} = f_o + \zeta/2, \quad (6)$$

where  $\zeta = \partial u / \partial y - \partial v / \partial x$  is the relative vorticity of the mesoscale flows (Weller 1982, Kunze 1985). Model simulations by Klein et al. (2004a,b) showed this effect clearly. The overall wind work does not appear to be substantially affected, but the lateral scales are reduced, acting in

concert with  $\beta$  to speed propagation out of the mixed layer. The  $\beta$  effect was dominant in the Ocean Storms Experiment (D'Asaro et al. 1995) (**Figure 8**), but in general, the mesoscale is likely an important modulator of the downward flux. This is apparent in **Figure 5**, where downward propagation varies significantly from year to year in spite of a fairly constant annual cycle of wind stress and a relatively weak mesoscale field.

## 6.2. Wave Refraction and Trapping

Once generated, propagating NIWs interact with the vorticity and shear of mesoscale motions in a variety of ways. Initial attempts to consider the interaction focused on ray tracing, which formally requires a scale separation between NIWs and mesoscale shear/stratification, assuming that the mesoscale provides a slowly varying medium with characteristic scales larger than the typical wavelength. For example, Kunze (1985) derived an approximate dispersion relationship for NIWs (essentially Equation 6) in the vorticity field of the eddies. A specific consequence is that the lowering of  $f_{\text{eff}}$  in anticyclonic eddies can trap NIWs, as observed in the Arctic by Halle (2003). Laterally sheared currents such as the Kuroshio and the Gulf Stream can also modulate  $f_{\text{eff}}$ ; Rainville & Pinkel (2004) observed significantly elevated NIW energy in the Kuroshio that appeared to be consistent with trapping.

Additionally, as vertical group velocity increases with frequency above  $f_{\text{eff}}$  (Equation 5), anticyclonic eddies can also create regions termed inertial chimneys, wherein locally lowered  $f_{\text{eff}}$  allows rapid deep propagation. First proposed by Lee & Niiler (1998), inertial chimneys also occur in numerical models (Zhai et al. 2005, 2007). Because eddies are typically surface intensified, the downward-propagating trapped waves can reach critical layers at the depth where the group velocity goes to zero as the background vorticity decreases. Although Kunze (1986) found some evidence of this process, observations of critical layers are very scarce.

The scales of eddies and NIWs are often of the same order, which violates the assumption of ray tracing, necessitating different approaches. A different but complementary approach is to consider interaction with a broad, statistically horizontally uniform field of geostrophic eddies. Young & Ben Jelloul (1997) introduced a theoretical framework for considering the slow amplitude evolution of NIWs propagating in a geostrophic eddy field. To do so, they relaxed the horizontal scale separation assumption implicit in the ray-tracing approach described above. Within this framework, and in subsequent work building on it (Balmforth et al. 1998, Balmforth & Young 1999), mesoscale vorticity essentially dephases near-inertial motions on eddy length scales, which subsequently allows them to more rapidly disperse. In the limit of eddy scales that are small compared with large-scale near-inertial motions, the net effect can be considered an enhanced effective dispersion, somewhat analogous to enhanced eddy diffusivity stemming from the effects of many small turbulent eddies acting on a large-scale scalar. Within the overall statistical result, there is some evidence from both analytic and numerical work that the vertical structure and degree of concentration/reduction of near-inertial energy may reflect the vorticity structure of the eddy field in ways that are similar to the inertial chimney ideas proposed earlier (Klein & Treguier 1995, Balmforth & Young 1999, Danioux et al. 2008). Analysis of satellite altimetry and surface drifters has observationally confirmed the general tendency of near-surface inertial motions to be organized by mesoscale vorticity (Elipot et al. 2010).

## 6.3. Nonlinear Wave-Mesoscale Interactions

The linear processes discussed above do not allow a reverse cascade to geostrophic motions or an energy exchange between them and NIWs. However, nonlinear interactions between NIWs

and mesoscale eddies have been posited theoretically (Müller 1976, Buhler & McIntyre 2005) and examined observationally (Brown & Owens 1981; Polzin 2008, 2010). In contrast to the near-inertial oscillation equation of Young & Ben Jelloul (1997), which explicitly rules out such transfers, the wave capture mechanism of Buhler & McIntyre (2005) allows for strong interactions when NIW packets are aligned with the strain field of the mesoscale flow. NIWs grow and gain energy at the expense of the eddy field when the strain exceeds the relative vorticity, or equivalently when the so-called Okubo-Weiss parameter changes sign. Polzin (2008, 2010) found some evidence for this process in a reinterpretation of data from the POLYMODE experiment but concluded that the transfer rates are smaller than those of other mechanisms that remove energy from the mesoscale eddy field, such as bottom drag. He further argued that three dimensionality and nonlinearity may call for caution in previous interpretations of wave-mesoscale interactions in terms of trapping and critical layers.

Stronger interactions may occur near fronts, where the gradients are stronger than they are in mesoscale eddies. For example, NIWs may play a role in catalyzing the wind-driven dissipation in fronts (D'Asaro et al. 2011, Thomas 2012, Whitt & Thomas 2013). Here, wind-driven NIWs interact strongly with the front such that their dispersion relationship is substantially altered (Whitt & Thomas 2013). The NIWs quickly become unstable, increasing local dissipation, and therefore appear to catalyze the transfer of energy from front to dissipation scales. Because the NIWs are wind generated, the wave-mean flow interactions are distinct from the spontaneous generation discussed above. Whether NIWs can radiate away from the front in these situations is unclear; additionally, the errors introduced into the wind work calculations by the presence of fronts are unknown (although modeling has suggested that they are small for weak fronts; Klein et al. 2004a). In sum, more observations and modeling are required to assess the importance and nature of these mechanisms. It is possible that submesoscale-NIW interactions represent a significant source of NIWs as well as a sink of mesoscale energy (Ferrari & Wunsch 2009).

## 7. MIXING

Near-inertial motions in the mixed layer result in shear across the transition layer that separates the mixed layer from the stratified waters below, which is a major mechanism for mixing and deepening of the mixed layer following storms (Plueddemann & Farrar 2006, Johnston & Rudnick 2009, Dohan & Davis 2011, Sanford et al. 2011). Although this mechanism is an aspect of NIW generation, it is not strictly a wave process and so is not reviewed here. We do note that the mixing and momentum transfer in the transition layer are not fully understood and are the subjects of active research.

In the ocean interior, NIWs have the potential to be more effective at mixing than internal tides as a result of variance at small vertical scales and their greater shear/strain ratio. Enhanced dissipation associated with NIWs has been measured by Fer (2014) in the Arctic (see sidebar Near-Inertial Waves in the Arctic), by Hebert & Moum (1994), and by Alford & Gregg (2001); **Figure 12** shows observations from this last study. Zonal shear  $U_z$  (**Figure 12a**) led meridional shear  $V_z$  (**Figure 12b**) by 90°, consistent with the counterclockwise rotation expected for the Southern Hemisphere. The phase propagation was upward, indicating downward energy propagation. Strain (**Figure 12c**), the vertical derivative of vertical displacement, also showed upward propagation. These observations indicated an NIW traveling downward from the surface. Microstructure observations (**Figure 12d,e**) showed enhanced diffusivity once each inertial period when the wave strain caused instantaneous stratification, and therefore the Richardson number  $Ri \equiv N^2/S^2$  (Howard 1961, Miles 1961) was the minimum. In this case, the minimum near-inertial Richardson

## NEAR-INERTIAL WAVES IN THE ARCTIC

The Arctic is a special environment for NIWs for two reasons: (*a*)  $\beta$  is nearly zero, such that the  $f$ -plane approximation is excellent, and (*b*) the seasonal cycle of wind forcing is extreme, with the ice providing insulation from wind forcing during the winter. As ice coverage decreases, feedbacks can potentially develop wherein the reduced amount of ice leads to more wind, more NIWs, more turbulence, and a greater upward flux of heat from the warm Atlantic waters below, which then leads to a further decrease in ice. Moored observations have shown extremely weak NIW kinetic energy under ice cover (Merrifield & Pinkel 1996, Rainville & Woodgate 2009, Martini et al. 2014); during the few times that turbulence under the ice has been measured, it was also much weaker than that at lower latitudes (Rainville & Winsor 2008), but NIWs have been tied to elevated mixing in the summer (Fer 2014).

number was approximately 0.6; shear at scales unresolved by the ADCP and/or other frequencies was assumed to lower the total Richardson number enough to trigger shear instability.

Additional evidence for the general importance of NIWs in mixing the upper ocean comes from analysis of parameterized diffusivities in the upper 500 m computed from Argo floats using the Gregg-Heney strain formulation (Whalen et al. 2012, 2015). The authors found strong seasonal cycles in certain latitude bands, with parameterized mixing several times higher in winter, suggesting that storm-generated NIWs enhance mixing. This hypothesis should be tested with more direct observations.

## 8. DISCUSSION

In spite of its ubiquity in ocean spectra, aspects of the near-inertial peak remain mysterious. There is little doubt that resonant wind forcing excites inertial mixed-layer motions that then propagate into the ocean interior. This connection between wind and interior NIWs can be seen in the form of local downward-propagating high-mode waves (Figures 4 and 5), a seasonal cycle in both upper- and deep-ocean near-inertial energy (Figure 6), and a loose geographic correlation between storm tracks, inertial mixed-layer motions, and low-mode equatorward-propagating energy (Figures 9 and 10). Yet several important parts of this particular story remain murky. To begin, the basic distribution of energy between low and high modes was not well measured by the Ocean Storms Experiment observations and has been poorly constrained by the few subsequent full-depth time series, especially at low latitudes. To the extent that low-mode waves may contain an appreciable percentage of the total energy [suggested theoretically by Gill (1984) and measured, at only two locations, by Alford (2010) and Silverthorne & Toole (2009)], their propagation pathways and lifetimes are largely unknown. D'Asaro et al. (1995) concluded that propagation of the first two modes accounted for all of the observed loss of depth-integrated energy but did not directly measure the flux. Observed fluxes from historical moorings in Figure 9 do show equatorward propagation, but how far do they go? The near-complete lack of full-depth data between 30°N and 30°S is frustrating. Modeled NIWs propagating from the storm tracks to the tropics result in spectral peaks that are blue-shifted well above the local  $f$  (figure 6 in Simmons & Alford 2012), which makes them easily distinguishable from locally forced motions. If NIWs indeed propagate that far from source regions, as the internal tides do, what is the fate of this long-propagating energy?

One of the most unclear (but undoubtedly important) issues is the role that mesoscale vorticity, shear, and strain play in setting (*a*) the initial resonant or near-resonant power transfer from the wind to the ocean, (*b*) the subsequent rate of conversion from purely inertial oscillations into propagating near-inertial internal waves, and (*c*) the subsequent propagation of the waves. NIWs

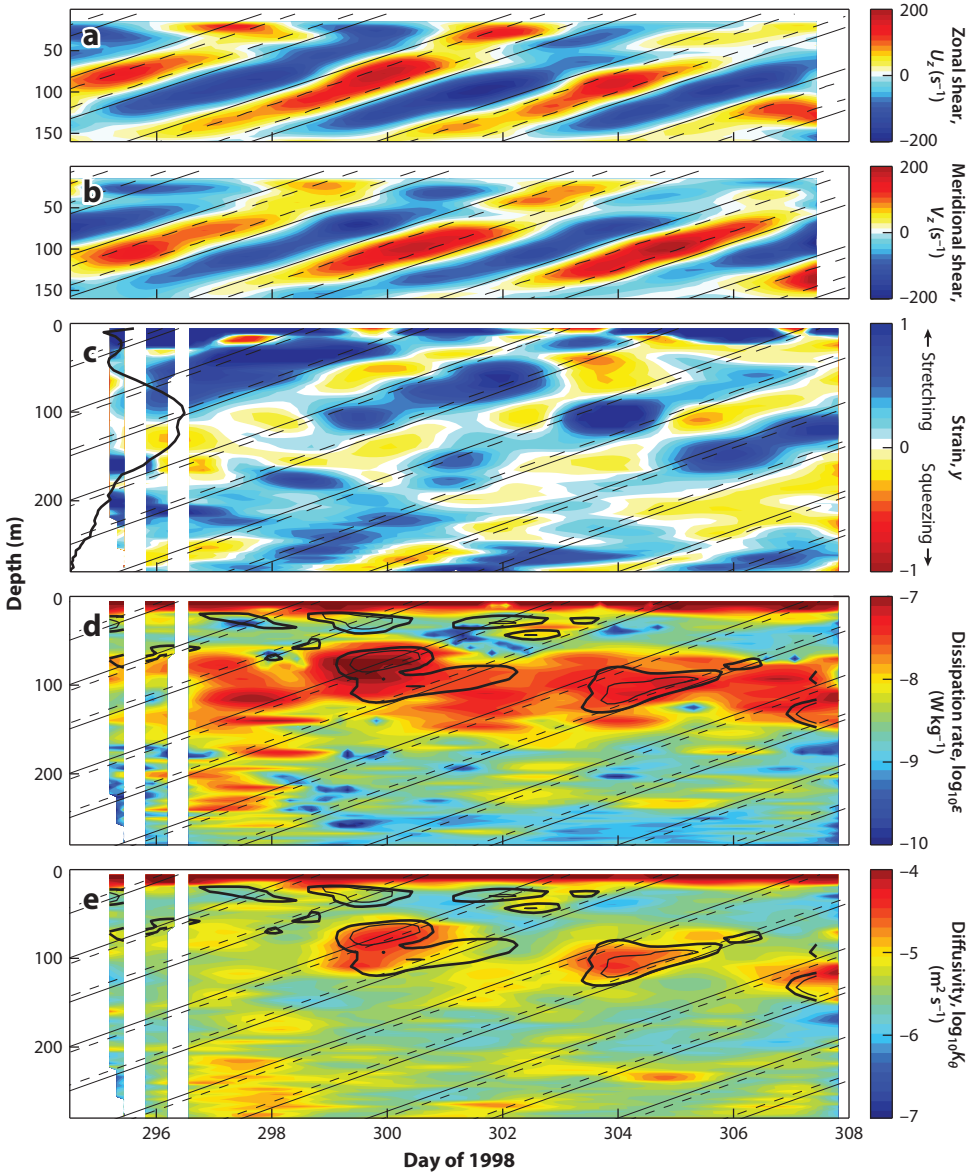


**Figure 12**

Observations of a near-inertial wave, showing two-day low-passed time/depth series of (a) zonal shear, (b) meridional shear, and (c) strain, along with (d) turbulent dissipation rate and (e) diffusivity from microstructure measurements. All quantities are plotted versus WKB-stretched depth, and plane wave solutions are overplotted with straight black lines. The mean buoyancy frequency profile is plotted to the left in panel c. Thick and thin contours in panels d and e indicate Richardson numbers of <1 and 0.64, respectively. Abbreviation: WKB, Wentzel, Kramers, Brillouin. Modified from Alford & Gregg (2001).

should be more affected by the mesoscale than are internal tides owing to their lower frequency (closer to the eddying timescales), shorter vertical scales, and slower propagation. Numerical and theoretical work discussed in Section 6 suggests an order-one influence, which has received some suggestive corroboration from global statistics (Eliopot et al. 2010). This topic appears ripe for further observational work.

Although it is clear that some of the near-inertial energy and shear in the ocean comes from the wind, it is not at all clear how much of it comes from this as opposed to other sources. Nonlinear wave-wave interaction, spontaneous generation, and internal lee-wave generation are all potential energy sources. Some form of observational evidence exists for each of these mechanisms, but the relative importance of them (and the geographical distribution of each) remains unknown.

One possible way to distinguish among the mechanisms is the upward/downward partition of energy flux. Propagation should be dominantly downward for wind-generated waves and upward for lee waves, and could be either direction for spontaneous imbalance and wave-wave interactions (although both of these should tend to increase toward the surface). Although downward energy does tend to exceed upward energy in the upper few hundred meters (Leaman & Sanford 1975) (**Figure 5**) and numerous observational examples exist of down-going shallow wave packets, up-going packets have also been observed, even in the deep ocean (Alford 2010). Additionally, recent analysis of the World Ocean Circulation Experiment (WOCE) lowered ADCP profiles suggests only a 20% excess of down-going energy in the upper 2,000 m (A.F. Waterhouse, J.A. MacKinnon, E. Kunze & R. Pinkel, manuscript in preparation). This could be evidence that the gravest few modes, which are equal parts up- and down-going, are dominant; alternatively, it could suggest a distributed importance of surface, midwater, and near-bottom mechanisms.

Useful metrics for comparing the relative importance of different mechanisms include both energetics and relevant timescales. In the case of the wind,  $O(0.5 \text{ TW})$  of power ( $P$ ) go into the NIW field, which in a steady state must be balanced by dissipation, giving a timescale of  $\tau = E/P$ , where  $E$  is the energy. Alford & Whitmont (2007) computed timescales of tens of days using moored records and a slab wind work model, which can be interpreted as the spin-down time if forcing were to stop. For comparison, low-mode waves could propagate across entire ocean basins in that time (Rainville & Pinkel 2006), whereas vertically propagating high-mode waves take months to reach the bottom of the ocean (Garrett 2001). The dissipation timescale of these waves is only a few days in high stratification (Gregg et al. 1986, Hebert & Moum 1994, Alford & Gregg 2001) but  $O(100 \text{ days})$  below the seasonal thermocline, where the Richardson number is stable (Alford & Gregg 2001). Hence, it may be that the 100–300-m shear features that are so ubiquitous and prominent are too slow to propagate to margins, where they can break, and not quite small enough vertically to break locally.

Over the past few decades, many studies have looked at the importance of turbulent mixing driven by internal tide breaking. The internal tide problem is comparatively a much easier one, because the internal tide generation map is comparatively well known, the tides' generation and propagation are somewhat deterministic (at least outside the coastal zone), and their sea surface height signature can be detected altimetrically. Significant effort has been put into developing parameterizations of enhanced turbulence caused by internal tide breaking (Jayne & St. Laurent 2001, Melet et al. 2013), which has significant effects on deep and abyssal circulation patterns and on the global meridional overturning circulation. Enhanced turbulence caused by NIW breaking may be equally important; however, because of their poorly understood generation, their temporal intermittency, and the possibly greater importance of mesoscale refraction and interaction, appropriate parameterizations of the full problem are still very much a work in progress. An initial sensitivity study by Jochum et al. (2012) involved generation through frequently coupled

winds (2 h) combined with an ad hoc vertical decay scale for NIWs and a lateral distribution similar to that in **Figure 9**. They found that the inclusion of turbulent mixing from near-inertial motions had a strong effect on tropical sea surface temperature and precipitation. Given that NIW mixing may be largely confined to the upper ocean, where heat is stored for later exchange with the atmosphere on seasonal and decadal timescales (timescales of interest to humans), the need to better understand the generation, propagation, and dissipation of NIWs looms large.

## DISCLOSURE STATEMENT

The authors are not aware of any affiliations, memberships, funding, or financial holdings that might be perceived as affecting the objectivity of this review.

## ACKNOWLEDGMENTS

The authors thank Tom Sanford, Eric D'Asaro, Mike Gregg, Chris Garrett, Rob Pinkel, and Bill Young for many helpful discussions, and to the many investigators and their technical staff who enabled the observations comprising our knowledge. This work was funded by the National Science Foundation and the Office of Naval Research.

## LITERATURE CITED

- Alford MH. 2001. Internal swell generation: the spatial distribution of energy flux from the wind to mixed-layer near-inertial motions. *J. Phys. Oceanogr.* 31:2359–68
- Alford MH. 2003a. Energy available for ocean mixing redistributed through long-range propagation of internal waves. *Nature* 423:159–63
- Alford MH. 2003b. Improved global maps and 54-year history of wind-work on ocean inertial motions. *Geophys. Res. Lett.* 30:1424–27
- Alford MH. 2008. Observations of parametric subharmonic instability of the diurnal internal tide in the South China Sea. *Geophys. Res. Lett.* 35:L15602
- Alford MH. 2010. Sustained, full-water-column observations of internal waves and mixing near Mendocino Escarpment. *J. Phys. Oceanogr.* 40:2643–60
- Alford MH, Cronin MF, Klymak JM. 2012. Annual cycle and depth penetration of wind-generated near-inertial internal waves at Ocean Station Papa in the northeast Pacific. *J. Phys. Oceanogr.* 42:889–909
- Alford MH, Gregg MC. 2001. Near-inertial mixing: modulation of shear, strain and microstructure at low latitude. *J. Geophys. Res.* 106:16947–68
- Alford MH, MacKinnon JA, Zhao Z, Pinkel R, Klymak J, Peacock T. 2007. Internal waves across the Pacific. *Geophys. Res. Lett.* 34:L24601
- Alford MH, Peacock T, MacKinnon JA, Nash JD, Buijsman M, et al. 2015. The formation and fate of internal waves in the South China Sea. *Nature* 521:65–73
- Alford MH, Shcherbina AY, Gregg MC. 2013. Observations of near-inertial internal gravity waves radiating from a frontal jet. *J. Phys. Oceanogr.* 43:1225–39
- Alford MH, Whitmont M. 2007. Seasonal and spatial variability of near-inertial kinetic energy from historical moored velocity records. *J. Phys. Oceanogr.* 37:2022–37
- Anderson DLT, Gill AE. 1979. Beta dispersion of inertial waves. *J. Geophys. Res.* 84:1836–42
- Arbic B, Shriner J, Hogan P, Hurlburt H, McClean J, et al. 2009. Estimates of bottom flows and bottom boundary layer dissipation of the oceanic general circulation from global high-resolution models. *J. Geophys. Res.* 114:C02024
- Balmforth NJ, Llewellyn Smith SG, Young WR. 1998. Enhanced dispersion of near-inertial waves in an idealized geostrophic flow. *J. Mar. Res.* 56:1–40

- Balmforth NJ, Young WR. 1999. Radiative damping of near-inertial oscillations in the mixed layer. *J. Mar. Res.* 57:561–84
- Brown E, Owens WB. 1981. Observations of the horizontal interactions between the internal wave field and the mesoscale flow. *J. Phys. Oceanogr.* 11:1474–80
- Buhler O, McIntyre M. 2005. Wave capture and wave-vortex duality. *J. Fluid Mech.* 534:67–96
- Cairns JL, Williams GO. 1976. Internal wave observations from a midwater float, 2. *J. Geophys. Res.* 81:1943–50
- Carter GS, Gregg MC. 2006. Persistent near-diurnal internal waves observed above a site of  $M_2$  barotropic-to-baroclinic conversion. *J. Phys. Oceanogr.* 36:1136–47
- Chaigneau A, Pizarro O, Rojas W. 2008. Global climatology of near-inertial current characteristics from Lagrangian observations. *Geophys. Res. Lett.* 35:L13603
- Chinn BS, Alford MH, Girton JB. 2012. Observations of internal waves and parametric subharmonic instability in the Philippines archipelago. *J. Geophys. Res.* 117:C05019
- Danioux E, Klein P, Riviere P. 2008. Propagation of wind energy into the deep ocean through a fully turbulent mesoscale eddy field. *J. Phys. Oceanogr.* 38:2224–41
- D'Asaro EA. 1985. The energy flux from the wind to near-inertial motions in the mixed layer. *J. Phys. Oceanogr.* 15:1043–59
- D'Asaro EA. 1989. The decay of wind-forced mixed layer inertial oscillations due to the  $\beta$  effect. *J. Geophys. Res.* 94:2045–56
- D'Asaro EA. 1995a. Upper-ocean inertial currents forced by a strong storm. Part II: modeling. *J. Phys. Oceanogr.* 25:2937–52
- D'Asaro EA. 1995b. Upper-ocean inertial currents forced by a strong storm. Part III: interaction of inertial currents and mesoscale eddies. *J. Phys. Oceanogr.* 25:2953–58
- D'Asaro EA, Eriksen CE, Levine MD, Niiler P, Paulson CA, Meurs PV. 1995. Upper-ocean inertial currents forced by a strong storm. Part I: data and comparisons with linear theory. *J. Phys. Oceanogr.* 25:2909–36
- D'Asaro EA, Lee C, Rainville L, Harcourt R, Thomas L. 2011. Enhanced turbulence and energy dissipation at ocean fronts. *Science* 332:318–22
- Dohan K, Davis RE. 2011. Mixing in the transition layer during two storm events. *J. Phys. Oceanogr.* 41:42–46
- Doherty K, Frye D, Liberatore S, Toole J. 1999. A moored profiling instrument. *J. Atmos. Ocean. Technol.* 16:1816–29
- Eden C, Olbers D. 2014. An energy compartment model for propagation, nonlinear interaction, and dissipation of internal gravity waves. *J. Phys. Oceanogr.* 44:2093–106
- Egbert GD, Ray RD. 2000. Significant dissipation of tidal energy in the deep ocean inferred from satellite altimeter data. *Nature* 405:775–78
- Ekman VW. 1953. *Studies on Ocean Currents: Results of a Cruise On Board the "Armauer Hansen" in 1930 Under the Leadership of Bjørn Helland-Hansen*. Geofys. Publ. Vol. 19. Bergen, Nor.: J. Griegs
- Elipot S, Lumpkin R, Prieto G. 2010. Modification of inertial oscillations by the mesoscale eddy field. *J. Geophys. Res.* 115:C09010
- Emanuel K. 2001. Contribution of tropical cyclones to meridional heat transport by the oceans. *J. Geophys. Res.* 106:14771–81
- Fer I. 2014. Near-inertial mixing in the central Arctic Ocean. *J. Phys. Oceanogr.* 44:2031–49
- Ferrari R, Wunsch C. 2009. Ocean circulation kinetic energy: reservoirs, sources, and sinks. *Annu. Rev. Fluid Mech.* 41:253–82
- Firing E, Lien RC, Müller P. 1997. Observations of strong inertial oscillations after the passage of Tropical Cyclone Ofa. *J. Geophys. Res.* 102:3317–22
- Ford R. 1994. Gravity wave radiation from vortex trains in rotating shallow water. *J. Fluid Mech.* 281:81–118
- Fu LL. 1981. Observations and models of inertial waves in the deep ocean. *Rev. Geophys. Space Phys.* 19:141–70
- Furuichi N, Hibiya T, Niwa Y. 2008. Model predicted distribution of wind-induced internal wave energy in the world's oceans. *J. Geophys. Res.* 113:C09034
- Garrett C. 2001. What is the “near-inertial” band and why is it different from the rest of the internal wave spectrum? *J. Phys. Oceanogr.* 31:962–71

- Garrett C, Munk WH. 1975. Space-time scales of internal waves: a progress report. *J. Geophys. Res.* 80:291–97
- Gerkema T, Shrira VI. 2005. Near-inertial waves on the “nontraditional”  $\beta$  plane. *J. Geophys. Res.* 110:C01003
- Gill AE. 1982. *Atmosphere-Ocean Dynamics*. San Diego, CA: Academic
- Gill AE. 1984. On the behavior of internal waves in the wake of a storm. *J. Phys. Oceanogr.* 14:1129–51
- Gregg M, D’Asaro E, Shay T, Larson N. 1986. Observations of persistent mixing and near-inertial internal waves. *J. Phys. Oceanogr.* 16:856–85
- Halle C. 2003. Internal wave variability in the Beaufort Sea during the winter of 1993/1994. *J. Geophys. Res.* 108:3210
- Hazewinkel J, Winters KB. 2011. PSI of the internal tide on a  $\beta$  plane: flux divergence and near-inertial wave propagation. *J. Phys. Oceanogr.* 41:1673–82
- Hebert H, Moum J. 1994. Decay of a near-inertial wave. *J. Phys. Oceanogr.* 24:2334–51
- Hoskins BJ, Bretherton FP. 1972. Atmospheric frontogenesis models: mathematical formulation and solutions. *J. Atmos. Sci.* 29:11–37
- Howard LN. 1961. Note on a paper of John W. Miles. *J. Fluid Mech.* 10:509–12
- Jayne SR, St. Laurent LC. 2001. Parameterizing tidal dissipation over rough topography. *Geophys. Res. Lett.* 28:811–14
- Jiang J, Lu Y, Perrie W. 2005. Estimating the energy flux from the wind to ocean inertial motions: the sensitivity to surface wind fields. *Geophys. Res. Lett.* 32:L15610
- Jochum M, Briegleb BP, Danabasoglu G, Large WG, Jayne SR, et al. 2012. On the impact of oceanic near-inertial waves on climate. *J. Clim.* 26:2833–44
- Johnston TMS, Rudnick DL. 2009. Observations of the transition layer. *J. Phys. Oceanogr.* 39:780–97
- Klein P, Lapeyre G, Large WG. 2004a. Wind ringing of the ocean in presence of mesoscale eddies. *Geophys. Res. Lett.* 31:L15306
- Klein P, Llewellyn-Smith S, Lapeyre G. 2004b. Organization of near-inertial energy by an eddy field. *Q. J. R. Meteorol. Soc.* 130:1153–66
- Klein P, Treguier AM. 1995. Dispersion of wind-induced inertial waves by a barotropic jet. *J. Mar. Res.* 53:1–22
- Komori N, Taguchi B, Ohfuchi W, Sasaki H, Klein P. 2008. Deep ocean inertia-gravity waves simulated in a high-resolution global coupled atmosphere-ocean GCM. *Geophys. Res. Lett.* 35:13–17
- Kroll J. 1975. The propagation of wind-generated inertial oscillations from the surface to the deep ocean. *J. Mar. Res.* 33:15–51
- Kunze E. 1985. Near-inertial wave propagation in geostrophic shear. *J. Phys. Oceanogr.* 15:544–65
- Kunze E. 1986. The mean and near-inertial velocity fields in a warm-core ring. *J. Phys. Oceanogr.* 16:1444–61
- Leaman KD, Sanford TB. 1975. Vertical energy propagation of inertial waves: a vector spectral analysis of velocity profiles. *J. Geophys. Res.* 80:1975–78
- Lee D, Niiler P. 1998. The inertial chimney: the near-inertial energy drainage from the ocean surface to the deep layer. *J. Geophys. Res.* 103:7579–91
- Lerczak JA, Winant CD, Hendershott MC. 2001. Observations and modeling of coastal internal waves driven by a diurnal sea breeze. *J. Geophys. Res.* 106:19715–29
- Lucas AJ, Pitcher GC, Probyn TA, Kudela RM. 2014. The influence of diurnal winds on phytoplankton dynamics in a coastal upwelling system off southwestern Africa. *Deep-Sea Res. II* 101:50–62
- Lvov YV, Polzin KL, Yokoyama N. 2012. Resonant and near-resonant internal wave interactions. *J. Phys. Oceanogr.* 42:669–91
- MacKinnon JA, Alford MH, Sun O, Pinkel R, Zhao Z, Klymak J. 2013. Parametric subharmonic instability of the internal tide at 29°N. *J. Phys. Oceanogr.* 43:17–28
- MacKinnon JA, Gregg MC. 2005. Near-inertial waves on the New England Shelf: the role of evolving stratification, turbulent dissipation, and bottom drag. *J. Phys. Oceanogr.* 35:2408–24
- MacKinnon JA, Winters KB. 2005. Subtropical catastrophe: significant loss of low-mode tidal energy at 28.9°. *Geophys. Res. Lett.* 32:L15605
- Martini KI, Simmons HL, Stoudt CA, Hutchings JK. 2014. Near-inertial internal waves and sea ice in the Beaufort Sea. *J. Phys. Oceanogr.* 44:2212–34

- McComas CH, Müller P. 1981. The dynamic balance of internal waves. *J. Phys. Oceanogr.* 11:970–86
- Melet A, Hallberg R, Legg S, Polzin KL. 2013. Sensitivity of the ocean state to the vertical distribution of internal-tide-driven mixing. *J. Phys. Oceanogr.* 43:602–15
- Merrifield MA, Pinkel R. 1996. Inertial currents in the Beaufort Sea: observations of response to wind and shear. *J. Geophys. Res.* 101:6577–90
- Mickett JB, Serra YL, Cronin MF, Alford MH. 2010. Resonant forcing of mixed layer inertial motions by atmospheric easterly waves in the northeast tropical Pacific. *J. Phys. Oceanogr.* 40:401–16
- Miles JW. 1961. On the stability of heterogeneous shear flows. *J. Fluid Mech.* 10:496–508
- Müller P. 1976. On the diffusion of momentum and mass by internal gravity waves. *J. Fluid Mech.* 77:789–823
- Müller P, Holloway G, Henyey F, Pophrey N. 1986. Nonlinear interactions among internal gravity waves. *Rev. Geophys.* 24:493–536
- Munk W, Phillips N. 1968. Coherence and band structure of inertial motion in the sea. *Rev. Geophys.* 6:447–72
- Munk W, Wunsch C. 1998. Abyssal recipes II: energetics of tidal and wind mixing. *Deep-Sea Res. I* 45:1977–2010
- Nagai T, Tandon A, Kunze E, Mahadevan A. 2015. Spontaneous generation of near-inertial waves from the Kuroshio Front. *J. Phys. Oceanogr.* 45:2381–406
- Nagasawa M, Niwa Y, Hibiya T. 2000. Spatial and temporal distribution of the wind-induced internal wave energy available for deep water mixing in the North Pacific. *J. Geophys. Res.* 105:13933–43
- Nam S, Send U. 2013. Resonant diurnal oscillations and mean alongshore flows driven by sea/land breeze forcing in the coastal Southern California Bight. *J. Phys. Oceanogr.* 43:616–30
- Nikurashin M, Ferrari R. 2010a. Radiation and dissipation of internal waves generated by geostrophic motions impinging on small-scale topography: application to the Southern Ocean. *J. Phys. Oceanogr.* 40:2025–42
- Nikurashin M, Ferrari R. 2010b. Radiation and dissipation of internal waves generated by geostrophic motions impinging on small-scale topography: theory. *J. Phys. Oceanogr.* 40:1055–74
- Nikurashin M, Ferrari R. 2011. Global energy conversion rate from geostrophic flows into internal lee waves in the deep ocean. *Geophys. Res. Lett.* 38:L08610
- Nikurashin M, Vallis GK, Adcroft A. 2013. Routes to energy dissipation for geostrophic flows in the Southern Ocean. *Nat. Geosci.* 6:48–51
- Niwa Y, Hibiya T. 1997. Nonlinear processes of energy transfer from travelling hurricanes to the deep ocean internal wave field. *J. Geophys. Res.* 102:12469–77
- Nowlin W Jr, Bottero J, Pillsbury R. 1986. Observations of internal and near-inertial oscillations at Drake Passage. *J. Phys. Oceanogr.* 16:87–108
- Pinkel R. 1985. A wavenumber-frequency spectrum of upper ocean shear. *J. Phys. Oceanogr.* 15:1453–69
- Plueddemann AJ, Farrar JT. 2006. Observations and models of the energy flux from the wind to mixed-layer inertial currents. *Deep-Sea Res. II* 53:5–30
- Pollard RT, Millard RC. 1970. Comparison between observed and simulated wind-generated inertial oscillations. *Deep-Sea Res.* 17:153–75
- Polzin KL. 2008. Mesoscale eddy-internal wave coupling. Part I: symmetry, wave capture, and results from the mid-ocean dynamics experiment. *J. Phys. Oceanogr.* 38:2556–74
- Polzin KL. 2010. Mesoscale eddy-internal wave coupling. Part II: energetics and results from PolyMode. *J. Phys. Oceanogr.* 40:789–801
- Polzin KL, Lvov YV. 2011. Toward regional characterizations of the oceanic internal wavefield. *Rev. Geophys.* 49:RG4003
- Price JF, Sanford TB, Forristall GZ. 1994. Forced stage response to a moving hurricane. *J. Phys. Oceanogr.* 24:233–60
- Rainville L, Pinkel R. 2004. Observations of energetic high-wavenumber internal waves in the Kuroshio. *J. Phys. Oceanogr.* 34:1495–505
- Rainville L, Pinkel R. 2006. Propagation of low-mode internal waves through the ocean. *J. Phys. Oceanogr.* 36:1220–36
- Rainville L, Winsor P. 2008. Mixing across the arctic ocean: microstructure observations during the Beringia 2005 expedition. *Geophys. Res. Lett.* 35:L08606
- Rainville L, Woodgate R. 2009. Observations of internal wave generation in the seasonally ice-free Arctic. *Geophys. Res. Lett.* 36:L23604

- Ray RD, Mitchum GT. 1996. Surface manifestation of internal tides generated near Hawaii. *Geophys. Res. Lett.* 23:2101–4
- Rimac A, von Storch JS, Eden C, Haak H. 2013. The influence of high-resolution wind stress field on the power input to near-inertial motions in the ocean. *Geophys. Res. Lett.* 40:4882–86
- Rossby C-G. 1938. On the mutual adjustment of pressure and velocity distributions in certain simple current systems, II. *J. Mar. Res.* 1:239–63
- Rudnick DL, Boyd TJ, Brainard RE, Carter GS, Egbert GD, et al. 2003. From tides to mixing along the Hawaiian Ridge. *Science* 301:355–57
- Sanford TB, Price JF, Girton JB. 2011. Upper-ocean response to Hurricane Frances (2004) observed by profiling EM-APEX floats. *J. Phys. Oceanogr.* 41:1041–56
- Scott R, Goff J, Garabato A, Nurser A. 2011. Global rate and spectral characteristics of internal gravity wave generation by geostrophic flow over topography. *J. Geophys. Res.* 116:C09029
- Shearman RK. 2005. Observations of near-inertial current variability on the New England shelf. *J. Geophys. Res.* 110:C02012
- Sherman JT. 1989. *Observations of fine scale vertical shear and strain in the upper ocean*. PhD Thesis, Univ. Calif., San Diego
- Silverthorne KE, Toole JM. 2009. Seasonal kinetic energy variability of near-inertial motions. *J. Phys. Oceanogr.* 39:1035–49
- Simmons HL. 2008. Spectral modification and geographic redistribution of the semi-diurnal internal tide. *Ocean Model.* 21:126–38
- Simmons HL, Alford MH. 2012. Simulating the long range swell of internal waves generated by ocean storms. *Oceanography* 25(2):30–41
- St. Laurent LC, Garabato ACN, Ledwell JR, Thurnherr AM, Toole JM, Watson AJ. 2012. Turbulence and diapycnal mixing in Drake Passage. *J. Phys. Oceanogr.* 42:2143–52
- Sun OM, Pinkel R. 2013. Subharmonic energy transfer from the semidiurnal internal tide to near-diurnal motions over Kaena Ridge, Hawaii. *J. Phys. Oceanogr.* 43:766–89
- Thomas LN. 2012. On the effects of frontogenetic strain on symmetric instability and inertia–gravity waves. *J. Fluid Mech.* 711:620–40
- Thurnherr AM, St. Laurent LC, Speer KG, Toole JM, Ledwell JR. 2005. Mixing associated with sills in a canyon on the midocean ridge flank. *J. Phys. Oceanogr.* 35:1370–81
- Tian J, Zhou L, Zhang X. 2006. Latitudinal distribution of mixing rate caused by the  $M_2$  internal tide. *J. Phys. Oceanogr.* 36:35–42
- Toole JM. 2007. Temporal characteristics of abyssal finescale motions above rough bathymetry. *J. Phys. Oceanogr.* 37:409–27
- van Haren H. 2005. Tidal and near-inertial peak variations around the diurnal critical latitude. *Geophys. Res. Lett.* 32:L23611
- Vanneste J. 2012. Balance and spontaneous wave generation in geophysical flows. *Annu. Rev. Fluid Mech.* 45:147–72
- Watanabe M, Hibiya T. 2002. Global estimates of the wind-induced energy flux to inertial motions in the surface mixed layer. *Geophys. Res. Lett.* 29:64–1–3
- Waterhouse AF, MacKinnon JA, Nash JD, Alford MH, Kunze E, et al. 2014. Global patterns of diapycnal mixing from measurements of the turbulent dissipation rate. *J. Phys. Oceanogr.* 44:1854–72
- Webster F. 1968. Observations of inertial-period motions in the deep sea. *Rev. Geophys.* 6:473–90
- Weller RA. 1982. The relation of near-inertial motions observed in the mixed layer during the JASIN (1978) experiment to the local wind stress and to the quasi-geostrophic flow field. *J. Phys. Oceanogr.* 12:1122–36
- Whalen CB, MacKinnon JA, Talley LD, Waterhouse AF. 2015. Estimating the mean diapycnal mixing using a finescale strain parameterization. *J. Phys. Oceanogr.* 45:1174–88
- Whalen CB, Talley LD, MacKinnon JA. 2012. Spatial and temporal variability of global ocean mixing inferred from Argo profiles. *Geophys. Res. Lett.* 39:L18612
- Whitt DB, Thomas LN. 2013. Near-inertial waves in strongly baroclinic currents. *J. Phys. Oceanogr.* 43:706–25
- Winters KB, Bouruet-Aubertot P, Gerkema T. 2011. Critical reflection and abyssal trapping of near-inertial waves on a  $\beta$ -plane. *J. Fluid Mech.* 684:111–36

- Wunsch C. 1998. The work done by the wind on the oceanic general circulation. *J. Phys. Oceanogr.* 28:2332–40
- Yang B, Hou Y. 2014. Near-inertial waves in the wake of 2011 Typhoon Nesat in the northern South China Sea. *Acta Oceanol. Sin.* 33:102–11
- Young W, Ben Jelloul M. 1997. Propagation of near-inertial oscillations through a geostrophic flow. *J. Mar. Res.* 55:735–66
- Zervakis V, Levine M. 1995. Near-inertial energy propagation from the mixed layer: theoretical considerations. *J. Phys. Oceanogr.* 25:2872–89
- Zhai X, Greatbatch RJ, Eden C. 2007. Spreading of near-inertial energy in a 1/12° model of the North Atlantic Ocean. *Geophys. Res. Lett.* 34:L10609
- Zhai X, Greatbatch RJ, Zhao J. 2005. Enhanced vertical propagation of storm-induced near-inertial energy in an eddying ocean channel. *Geophys. Res. Lett.* 32:L18602
- Zhao Z, Alford MH. 2009. New altimetric estimates of mode-1  $M_2$  internal tides in the central North Pacific Ocean. *J. Phys. Oceanogr.* 39:1669–84
- Zhao Z, Alford MH, Girton JB. 2012. Mapping low-mode internal tides from multisatellite altimetry. *Oceanography* 25(2):42–51

## Contents

Global Ocean Integrals and Means, with Trend Implications <i>Carl Wunsch</i> .....	1
Visualizing and Quantifying Oceanic Motion <i>T. Rossby</i> .....	35
Cross-Shelf Exchange <i>K.H. Brink</i> .....	59
Effects of Southern Hemisphere Wind Changes on the Meridional Overturning Circulation in Ocean Models <i>Peter R. Gent</i> .....	79
Near-Inertial Internal Gravity Waves in the Ocean <i>Matthew H. Alford, Jennifer A. MacKinnon, Harper L. Simmons, and Jonathan D. Nash</i> .....	95
Mechanisms of Physical-Biological-Biogeochemical Interaction at the Oceanic Mesoscale <i>Dennis J. McGillicuddy Jr.</i> .....	125
The Impact of Submesoscale Physics on Primary Productivity of Plankton <i>Amala Mahadevan</i> .....	161
Changes in Ocean Heat, Carbon Content, and Ventilation: A Review of the First Decade of GO-SHIP Global Repeat Hydrography <i>L.D. Talley, R.A. Feely, B.M. Sloyan, R. Wanninkhof, M.O. Baringer, J.L. Bullister, C.A. Carlson, S.C. Doney, R.A. Fine, E. Firing, N. Gruber, D.A. Hansell, M. Ishii, G.C. Johnson, K. Katsumata, R.M. Key, M. Kramp, C. Langdon, A.M. Macdonald, J.T. Mathis, E.L. McDonagh, S. Mecking, F.J. Millero, C.W. Mordy, T. Nakano, C.L. Sabine, W.M. Smethie, J.H. Swift, T. Tanhua, A.M. Thurnherr, M.J. Warner, and J.-Z. Zhang</i> .....	185
Characteristic Sizes of Life in the Oceans, from Bacteria to Whales <i>K.H. Andersen, T. Berge, R.J. Gonçalves, M. Hartwig, J. Heuschele, S. Hylander, N.S. Jacobsen, C. Lindemann, E.A. Martens, A.B. Neubeimer, K. Olsson, A. Palacz, A.E.F. Prowe, J. Sainmont, S.J. Traving, A.W. Visser, N. Wadhwa, and T. Kiørboe</i> .....	217

Mangrove Sedimentation and Response to Relative Sea-Level Rise <i>C.D. Woodroffe, K. Rogers, K.L. McKee, C.E. Lovelock, I.A. Mendelsohn, and N. Saintilan</i> .....	243
The Great <i>Diadema antillarum</i> Die-Off: 30 Years Later <i>H.A. Lessios</i> .....	267
Growth Rates of Microbes in the Oceans <i>David L. Kirchman</i> .....	285
Slow Microbial Life in the Seabed <i>Bo Barker Jørgensen and Ian P.G. Marshall</i> .....	311
The Thermodynamics of Marine Biogeochemical Cycles: Lotka Revisited <i>Joseph J. Vallino and Christopher K. Algar</i> .....	333
Multiple Stressors in a Changing World: The Need for an Improved Perspective on Physiological Responses to the Dynamic Marine Environment <i>Alex R. Gunderson, Eric J. Armstrong, and Jonathon H. Stillman</i> .....	357
Nitrogen and Oxygen Isotopic Studies of the Marine Nitrogen Cycle <i>Karen L. Casciotti</i> .....	379
Sources, Ages, and Alteration of Organic Matter in Estuaries <i>Elizabeth A. Canuel and Amber K. Hardison</i> .....	409
New Approaches to Marine Conservation Through the Scaling Up of Ecological Data <i>Graham J. Edgar, Amanda E. Bates, Tomas J. Bird, Alun H. Jones, Stuart Kininmonth, Rick D. Stuart-Smith, and Thomas J. Webb</i> .....	435
Ecological Insights from Pelagic Habitats Acquired Using Active Acoustic Techniques <i>Kelly J. Benoit-Bird and Gareth L. Lawson</i> .....	463
Ocean Data Assimilation in Support of Climate Applications: Status and Perspectives <i>D. Stammer, M. Balmaseda, P. Heimbach, A. Köhl, and A. Weaver</i> .....	491
Ocean Research Enabled by Underwater Gliders <i>Daniel L. Rudnick</i> .....	519

## Errata

An online log of corrections to *Annual Review of Marine Science* articles may be found at  
<http://www.annualreviews.org/errata/marine>